Laser micro/nano-structuring pushes forward smart sensing: Opportunities and challenges

Yabin Zhang,[1] Xiangyu Wang,[1,2] Kai Yan,[3] Hai Zhu,[4,*] Ben Wang,[2,*] Bingsuo Zou[1,*]

1 Guangxi Key Laboratory of Processing for Non-Ferrous Metals and Featured Materials, School of Resource, Environments and Materials, Guangxi University, Nanning 530004, China (zoubs@gxu.edu.cn)

2 College of Chemistry and Environmental Engineering, Shenzhen University, Shenzhen 518055, China (benwang@szu.edu.cn)

3 College of Bioresources Chemical and Materials Engineering, Shaanxi University of Science and Technology, Xi'an 710021, China

4 Department of Civil Engineering, The University of Hong Kong, Pokfulam, Hong Kong SAR 999077, China (zhuhai@hku.hk)

Abstract

Post-pandemic era poses an imperative demand on progressive sensing devices whose performance largely relies on the morphologies and structures of sensing materials. Despite substantial efforts and advances have been made in sensing materials with different micro/nanoscale dimensionalities, it is still challenging to couple micro/nano platforms with sensing materials together for the precise and scalable production of high-performance sensors towards practical application scenarios. Owing to noncontact, precise, and high-efficiency features, laser micro/nanofabrication offers a promising solution to achieve high-quality micro-/nano sensors with novel functionalities in a relatively short time. Herein, this review begins with a glance over the development of micro/nano-structured sensors, and briefly discusses the importance of laser micro/nanostructuring technology for micro/nano-engineering of the sensors. Next, representative processing methods are elaborated in detail from a laser-pulse-type point of view, with potential applications towards chemical, physical, and biological targets based on different sensing mechanisms summarized. Finally, the perspectives on the opportunities and challenges of laser micro/nanostructuring strategies and materials for micro/nanosensors are presented.

Keywords: Laser micro/nanofabrication, Micro/nano-structuring sensors, Chemical sensing, Physical sensing, Biosensing

1. Introduction

With the advent of the intelligent era, the ecosystem of IoT and big data needs countless sensors for perceiving, acquiring, and detecting information, making the sensors one of the most important interfaces connecting human and machine as well as things and things. A multitude of sensors are embedded in commercially available smartwatches, smart clothing, and virtual/augmented reality devices to monitor the body or the surrounding environment. These sensors can convert physical, chemical, biological and other signals collected into easily identifiable signals like electrical or optical ones, thus being employed for the smart control of household appliances, environmental monitoring, and human activity tracking.[1-2] More remarkably, the prevalent COVID-19 epidemic imperatively needs high-performance smart biosensors, accelerating the fast-moving development of sensors with fast, real-time and remote monitoring ability.[3] As demonstrated, the device functions can be enhanced through regulating its surface chemical composition,[4] structure,[5] and materials lattice structure in varied spatial scales.[6] Thus, it is of paramount importance to enhance the performance of sensors through surface micro-/nanoscale engineering proved effectively by as-explored applications in sensing materials design.[1,7-10] Micro/nano sensors have cut a striking figure in the IoT and biomedical industries due to their small size, light weight, high sensitivity, low power consumption, massive measurement, and low cost. The control in feature sizes and morphologies of the designed micro-/nanoscale structures could better boost the properties. Recent years have witnessed the introduction of rich variations in micro/nanostructure dimensionality for improving the detection range, sensitivity, selectivity, and response speed.[11-15] Although micro/nanotechnology has been applied widely for designing sensing materials to improve the detection limit to ppm level and even ppb level, poor size control leads to the uncontrollability and unrepeatability of the sensor performance.[16,17] How to integrate micro/nanostructures seamlessly and precisely into sensing materials and to simultaneously reserve both merits has become a key issue, which is promoting a new micro/nanostructuring strategy for high-performance micro/nano sensors.

Benefiting from the advance in functional micro/nanostructured surfaces, diverse micro/nano processing techniques, such as etching, sol-gel, vapor deposition, electrochemical processing, template synthesis, photolithography, nanoimprinting, and printing, have been developed for micro/nanostructuring sensing materials.[18-21] Each technology has its own unique advantages

for different scenarios, such as high precision, high quality, good performance, and large-area fabrication as well as specific usage. Unfortunately, the requirement of expensive or special equipment, complex process, high cost, tedious period, and limited precision and resolution cannot be ignored when fabricating micro/nanoscale devices. These methods fail to meet the growing requirements of the trend of miniaturization, precision, integration, and customization for higher-efficient, higher-precise, and more controllable micro/nano sensors. It is still imperative for new strategies for constructing micro/nanostructures in/on sensing materials in efficient, accurate, and facile way. Recently, laser processing has attracted significant attention due to its ultrahigh processing accuracy, simplicity, rapidity, excellent controllability, environment friendly, and broad applicability for a wide range of materials, which opens up a new avenue for additive manufacturing and micro/nano-fabrication techniques. As an efficient noncontact strategy, it is a significantly advanced technique for high-quality micro/nanostructure through changing the surficial physical state and properties of materials with laser radiation, finally achieving shape and size control across multiple scales for sensors,[22] semiconductor devices,[23] micro-/nanofluidics,[24,25] flexible electronics,[26,27] and catalysts.[28,29] Compared to traditional manufacturing methods, it shows distinct physical effects and interaction mechanism, especially exhibiting good ability and processing quality of sophisticated and complex structures as well as high reproducibility. Using a high-energy laser beam for materials ablation enables the surface texturing of sensing materials. Various sensing materials have so far been prepared selectively by laser ablation, laser sintering, laser annealing, laser reduction, laser deposition, and laser-induced hydrothermal reaction.[30-32] Most importantly, laser micro/nano-structuring treatment can realize the surface modifications of sensing materials, especially the formation of micro/nanostructures with a high surface area offering more active active sites as well as the effective conversion of surface chemistry into more active components in different materials. Moreover, regular or periodic nanostructures on the surface may bring up novel physical effects like local field or change the surface potential and its spatial distribution. Such structural or compositional variations and their cooperations could accelerate the interaction of sensing materials with analytes or stimuli and amplify the conversion of generated signals, from both chemistry or physics, finally offering the possibility for the optimization and improvement of sensor performance.[1,7,19,22,33,34] Accordingly, a wide range of sensors based on laser-texturing micro/nanostructures have been achieved and

explored extensively, which is being used in wearable devices towards biomedicine, energy, and environment field. The continuous innovation of laser micro/nanofabrication will fuel the progress on making sensor smarter.

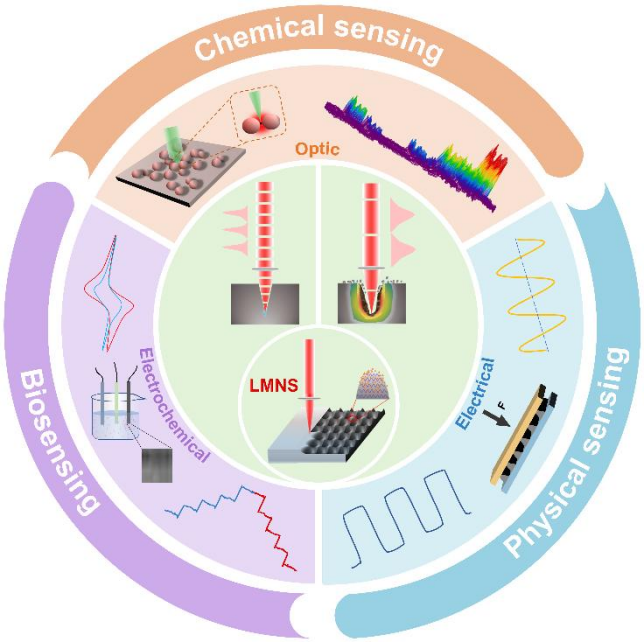

Figure 1. Schematic illustration of laser micro/nano structuring (LMNS) with short and long-pulsed lasers for chemo-/bio-/physical sensing applications based on the changes of optical, electrical, and electrochemical signals through utilizing widely existing surface enhanced Raman effect, electrochemical reaction, chemoresistance, piezoelectricity, piezo-resistance, and so on.

Based on extensive progress in micro/nano sensors and benefiting from laser micro/nanofabrication, the preparation of sensing materials, the assembly of sensing devices, and the improvement in sensing performance have further explored and innovated, thus boosting the sensing industry. In the following sections, a broad picture of the research is presented on laser micro/nanostructuring for chemo-/bio-/physical sensing applications based on the understanding of potential sensing mechanisms, as illustrated in **Figure 1**. All of the research activities are comprehensively and thoughtfully discussed on the utilization of laser-micro/nanostructuring technology to realize a wide range of micro/nano sensors for detecting various chemical, physical, and biological targets. This review exhaustively covers the concrete summary of multiple laser processing strategies based on the laser pulse type and the elaboration of sensing applications of laser micro/nanostructuring materials on the basis of sensing mechanisms. Finally, this review provides a critical analysis of laser micro/nanostructuring materials for micro/nano sensors and insights into remaining challenges

and future directions. With worldwide efforts, innovations in laser-texturing micro/nanostructures elaborated in this review may push forward the frontiers of micro/nano sensors with high performance, which will revolutionize the future sensing industry.

2. Laser micro/nanostructuring strategies

Since the establishment of the first functional laser by Theodore H. Maiman at the Hughes Research Laboratory in 1960,[35] it has opened a widespread field with diverse applications. Due to its high power, good spatial and temporal coherence over traditional light sources, the laser could be easily focused into a tiny spot or point for treating materials. Because illuminated local parts become removal by photochemical reaction and atomic bond breaking,[36] microscale or sub-microscale structures are formed ultimately. As reported successively by Srinivasan et al. in 1982 and 1986, 193 nm pulsed laser (tens of nanoseconds or picoseconds) was used for etching the surface of PET, PMMA, and PI.[37,38] The resultant micro-processing and nano-manufacturing technology possess better resolution and uniformity, attracting extensive attention for the fabrication of micro/nano structures. With the exploration going deeply, the comprehensive understanding in physical mechanisms of laser micro/nanomanufacturing enables the preparation of structures with controlled morphology and good quality. Most previous reviews have been summarized for growing and fabricating 1D, 2D, and 3D nanomaterials as well as micro/nanostructures.[39-41] To obtain the desired performance, the laser processing parameters like laser wavelength, pulse duration, laser power, and repetition frequency are of great significance and should be considered. As one of two important parameters evaluating lasers, laser pulse duration, regarded as full-width at half of the maximum amplitude of the laser pulse, is a vital parameter directly controlling the topography and microstructural changes as well as the final performance of the treated materials. In general, laser pulse duration regimes for laser material processing are classified into two types. One is the long pulse duration ranging from nanosecond to millisecond, generating quite a significant HAZ in the material due to its interaction with the material lattice. Another is the short pulse duration involving picosecond to femtosecond, whose thermal diffusion can be limited and neglected due to only interaction of short pulse laser with electrons.[42] Based on this simple category, the lasers with long or short pulse durations have been used to fabricate different micro/nanomaterials. When long-pulsed laser or even continuous wave laser irradiate on the materials, the target material is continuously heated. Then the laser pulse energy is spread

by heat conduction to an area outside the laser spot size, producing an uncontrollable melt layer due to the boiling and evaporation of the treated material. So, there are a series of thermal processes during the laser-materials interaction, including heat diffusion, melting and vaporizing, and melt expulsion induced by vapor pressure. The melt expulsion is mainly responsible for material removal mechanism of long-pulsed laser processing owing to an uncontrollable melt layer or zone.[43] This interaction mechanism results in poor surface quality like unavoidable recast material layer, thermal and mechanical damages, and HAZ. To improve the surface quality, long-pulsed laser parameters are optimized intricately.

Table 1. Comparison of laser manufacturing with respective to the laser with different pulse durations.

	Millisecond	**Nanosecond**	**Picosecond**	**Femtosecond**
Wavelength (nm)	1064	355, 1064	515, 532, 1030, 1064	800, 1030
Pulse length FWHM (s)	10-3	10-9	10-12	10-15
Scanning speed (mm/s)	10- 1000	0.1-800	2.4-3000	0.01-500
Spot size (μm)	1.06 -125	5-500	1-125	12-120
Structure types	Craters, holes, grooves and their patterns, sub-microparticles	Microgrooves/columns/ holes/grids/pits, sub-microgrooves, nanoparticles	Micro-grooves/columns/ holes/cubes/grids/pits, nanoparticles, periodic nanostructures, nano-ripples/wires/spheres, nanoporous structures, irregular nanostructures	Microgrooves/holes/ columns/cubes/grids/pits, nanoparticles, periodic nanostructures, nano-ripples/wires/holes/spheres, nanoporous structures, irregular nanostructures
Geometry resolution (μm)	Width: 200 Height: 15	Width: 10 Height: 3	Width: 5 Height: 2	Width: ≤5 Height: ≤1
Equipment cost	Low	Low	High	Highest
Processing cost	Low	Low	Low	Low
Processing time	Tens of mins	20-45 min	30s-10 min	30s-5 min
Applied Materials	Metals, glass, polymers	Metals, few ceramics, glass, polymers	All type	All type
Applications	Laser drilling Heat treatment	Laser micro-structuring, Laser rapid prototyping, Laser marking	Laser micro/nanostructuring, Precise medicine, Precise processing,	Laser micro/nanostructuring, Precise medicine, Precise processing,

In contrast, short-/ultrashort-pulsed lasers ablate targeted material within a spatial or well-defined area with minimized mechanical and thermal damage, suitable for high-precision micro- and nanomachining. Due to the extremely short interaction time accompanied by a much smaller thermal diffusion length, the materials are directly evaporated by strong Coulomb repulsion forces because of the generation and acceleration of a large number of free electrons and the unchanged positions of the ionized lattice atoms. The corresponding mechanism of material removal is attributed to phase explosion. This removal mechanism could achieve the control over surface topography, thus easily generating micro/nanostructured surfaces for further functionalization. It is demonstrated that the precise laser processing can be achieved by a laser with pulse durations of 10 picosecond or less.[44] Based on the laser-materials interaction features and removal mechanism, millisecond (ms), nanosecond (ns), picosecond (ps), and femtosecond (fs) laser processing have been distinguished and extensively used for a diversity of laser-machining process of various micro/nano sensors based on the key laser parameter.[45-47] Their outstanding features also embody in the process of laser annealing such as synthesis and carbonization, which have been explored and summarized everywhere. We compared their pros and cons in Table 1 and elaborated on specific examples in the following section.

2.1 Millisecond lasers

Due to huger energy, long pulse duration, and competent rate of materials removal, millisecond laser processing has been used widely for cutting or drilling, especially in high-speed drilling fields without the requirement of relatively high precision.[48,49] However, it often results in undesirable defects such as recast layer, oxidized layers, heat-affected/thermomechanical-affected zones, and spatter. When used for surface texturing or structuring, high-energy laser beam could cause target surface to be partially melted and eject molten material from the dimple because of the increasing heating and cooling cycle during extended pulse irradiation, finally leading to thermal damage of the target. To alleviate the heat accumulation caused by long-pulsed laser, Zhou et al. constructed a series of laser-texturing microstructures of about 500-700 μm in diameter on 304 stainless steels in air and underwater using a long-pulsed millisecond laser (0.2 ms, 1070 nm, < 1500 W) to investigate the effect of laser power, pulse number and water layer on the morphology and ablation volume (Figure 2a).[50] They found that the liquid-assisted ablation showed up to four times higher ablation volume than that in air due to

additional mechanical impact and produced a more regular laser-textured microstructure. To further improve the machining quality using the conventional millisecond laser, the pulse duration is controlled as low as possible (1 ms), and the combined pulse laser is explored.[51] Zhu et al. established 2D numerical model to analyze the influence of laser processing parameters on a crater feature and a melted zone and verified it by experiments.[52] The results showed that laser peak power density and pulse duration greatly affected the depth and diameter of the crater. With increasing pulse duration after 1.5 ms, the height of the edge bulge decreased. Moreover, a longer laser duration resulted in a larger melted zone for the same depth. Jia et al. utilized a novel combined pulse laser composed of an initial nanosecond pulse (1064 nm, 17 ns, 400 W) and a millisecond pulse (1070 nm, 0.1-5 ms, 800 W) for drilling the alumina ceramic.[53] The initial use of nanosecond pulse laser introduced a keyhole with a depth of 21.5 μm, greatly reducing the diameter below 200 μm and cracks of the final hole obtained by the subsequent treatment of millisecond pulse laser (Figure 2b). This verified that the synergy of the millisecond laser and other pulsed laser effectively enhanced the processing quality. In recent years, the improved millisecond laser manufacturing has been applied to construct a series of micro/nanostructures with various shapes and sizes on different materials with desired performance owing to its cheaper and faster features.[54-56] However, few studies have been reported on the application of millisecond pulsed laser-texturing for the fabrication of the micro/nano sensors. As reported recently, nanomaterials like nanoparticles with defect-rich surfaces obtained by a liquid-assisted laser ablation show promise in detecting gases at room temperature.[57-59] For example, Mintcheva et al. used millisecond pulsed laser (1064 nm, 1 ms, 5000 W) to irradiate TiO_2 nanopowder, finally obtaining spherical TiO_2 nanomaterials with average diameter of ~106 nm.[60] When gold nanoparticles with average size of 10.8 nm and 14.4 nm were decorated on them, the resulting nanocomposites could selectively detect ammonia, acetaldehyde and benzene. Excellent gas sensing ability was attributed to the formation of surface Ti^{3+} species and oxygen vacancies by laser irradiation. In a word, as a thermal-based process, millisecond laser machining is cheaper and faster, but the mechanism of local heating is accompanied by typical thermal defects like recast layer or heat affected zones ranging from 50 to 500 mm.[61-63] Moreover, it usually achieves the microstructure construction on the substrate due to the space effect of heating and thermal process, suffering from a significant limitation in the improvement of sensing performance.

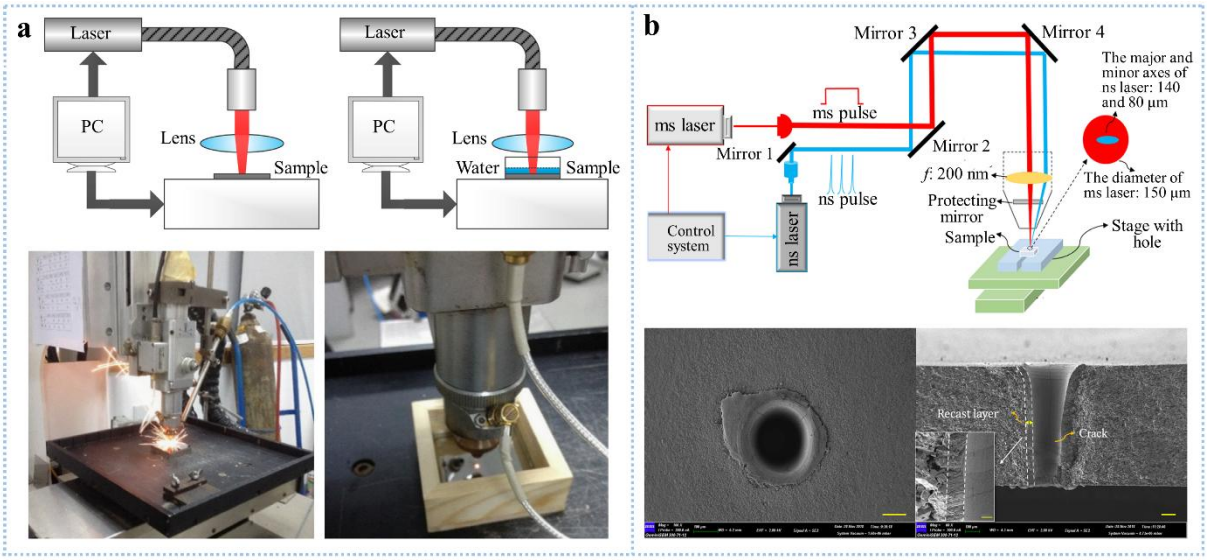

Figure 2. Millisecond laser processing. a) The schematic and actual processing of laser-microstructuring 304 stainless steel in air and underwater using a long-pulsed laser of 0.2 ms. Reproduced with permission.[50] Copyright 2016, Elsevier. b) The schematic diagram of the experimental system consisting of a millisecond laser modulated by a 1070 nm CW laser and a 1064 nm nanosecond laser, which drilled the hole with a well quality and only few tiny cracks found in the inner wall. Reproduced with permission.[53] Copyright 2020, Elsevier.

2.2 Nanosecond lasers

As a kind of long-pulsed laser with lower energy and reduce duration, nanosecond laser is one of the most common lasers for laser micro/submicro-structuring of target surfaces.[64,65] A pulse width on the order of nanosecond enables this manufacturing technology to remove excess material because enough pulse time conduces to the propagation of thermal wave into the treated substrate to produce a relatively more molten layer. Similar to millisecond laser processing, it also ejects the substrate material in the form of liquid and vapor due to a recoil pressure and vaporization and creates an uncontrollable melt layer owing to the melting and evaporation of the substrate.[43] Nevertheless, ultrashort pulse duration makes its HAZ smaller. Accordingly, this technique has been widely employed in the field of microfabrication, achieving a variety of biomimetic micro-/submicro-structured materials with different functions like wear resistance, water/frost/ice resistance, and corrosion resistance.[66-69] Until now, several studies have emerged on the application of nanosecond pulsed laser for constructing microstructures in a wide range of substrate materials.[70,71] Recent years have witnessed the fabrication of hierarchical structures on substrates submerged in a liquid medium by utilizing nanosecond laser structuring, which greatly enhance the sensing performance.[72,73] Moreover,

different processing parameters have been explored to control or realize the laser-texturing structures and properties for desired sensing ability. To overcome the challenge encountered by surfactant-free fabrication and patterning of rGO micro/nanostructures for high-performance sensing device, Guo et al. used a single-mode Nd:YAG nanosecond laser (10 ns, 0.1-0.3W) to fabricate rGO stripes of 200 nm in width for patterned hierarchical nanostructures to sensing humidity (Figure 3a).[74] Due to the tuned conductivity from laser reduction together with the improved guest molecular adsorption, the micro/nanostructured rGO displayed excellent sensitivity to humidity, fast and tunable response/recovery time. Considering cost-effectiveness and fast processing times for real industrial requirements, Ta et al. utilized nanosecond laser (1064 nm, 220 ns, 55-93 J/cm^2) to pattern copper and brass surfaces for chemical sensing (Figure 3b).[75] The wettability of the laser-pattered surfaces composed of microgrooves of 75 μm in width and 10-25 μm in depth changed with the methanol concentration in a solution, making it a novel chemical sensor. Compared with ultrafast laser systems like picosecond laser processing, this technology offered a low-cost, robust, and time-effective system. Combining tightly focused nanosecond pulsed laser (532 nm, 7 ns, 2-15 nJ) with an accelerated Ar^+ beam, Kuchmizhak et al. fabricated isolated plasmonic nanorods of 300-500 nm, separated and merged nanorings of 0.5-3 μm, as well as more complex nanorod-nanoring assembles on glass substrates (Figure 3c).[76] The first irradiation with nanosecond laser initiated fast melting and subsequent hydrodynamic processes. After Ar^+ polishing, LSPR-supporting isolated plasmonic structures on the substrate are produced. Their average diameter and height increase with pulse energy increasing, suggesting that laser pulse energy affects the size of plasmonic structures to dominate the LSPR-sensing behavior. To integrate precise and durable sensors on orthopedic implants, Hu et al. used a 355 nm UV nanosecond laser with a pulse duration of 25 ns and a output power of 5.5 W to directly prepare sensors on the CFR-PEEK parts (Figure 3d).[77] The control in laser parameters like scan speed could optimize the morphology from flakes to flocculent form, chemistry, and conductivity of laser annealed CFR-PEEK (LACP), thereby achieving strain sensors with superior linearity (R^2 = 0.997) over the loading range (0-2.5% strain). Even if being mounted on irregular and complex implants such as hip joints, they still showed good segmented linear response and GF within 0-0.29% strain. Moreover, this sensor could integrate with a Bluetooth module, showcasing great promise in digitalized medical devices and personalized smart orthopedics. Despite some advances regarding nanosecond laser

surface texturing, the textured structure or pattern gets an oval shape in case of square texturing. Due to heating action by a long laser pulse, it is best suitable for higher thickness substrate. To sum up, nanosecond laser processing with reliable source and low-cost operation is gradually maturing. The easy formation of obvious HAZ, the production of recast materials, or the delamination and cracking of surface textured structures limit its application in high-precision machining, which needs to be improved and solved in near future via further technology innovation and combination.

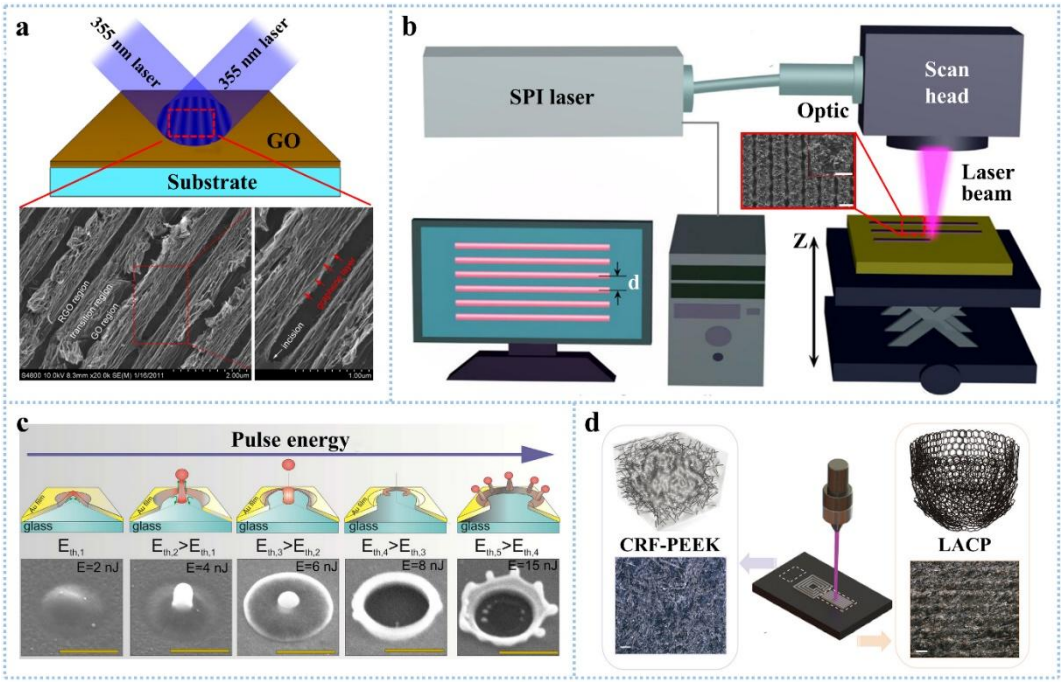

Figure 3. Nanosecond laser microstructuring processing. a) The fabrication schematic and morphology of rGO hierarchical nanostructures by TBLI reduction and patterning with 10 ns laser of 0.1-0.3 W for humidity sensing. Reproduced with permission.[74] Copyright 2012, Elsevier. b) Fabrication schematic and resultant morphology of microgroove structures on copper and brass surfaces by using a laser with the pulse width of~220 ns. Reproduced with permission.[75] Copyright 2015, the authors, published by Elsevier. c) Fabrication illustrations of functional plasmonic nanostructures by texturing a noble metal film on a glass substrate by using a single tightly focused nanosecond pulse laser at different pulse energies as well as the corresponding SEM images of the resolidified nanostructures on the 75-nm-thick Au film surface. Reproduced with permission.[76] Copyright 2016, the authors, published by Springer Nature. d) The direct writing schematic of LACP-based sensor with a UV nanosecond laser of 355 nm and the corresponding morphology obtained by controlling laser parameters. Reproduced with permission.[77] Copyright 2022, the authors, published by Wiley-VCH.

2.3 Picosecond laser

Compared with long-pulse laser processing stated above, short-/ultrafast-pulse(femto-/pico-second) laser processing possesses the relatively low pulse energy, shorter pulse width, and ultrahigh peak power.[45,78] As one kind of ultrafast laser processing, picosecond laser processing possesses less thermal damage, high precision and fast-speed reaction owing to direct atom destruction in materials caused by the ultrahigh energy density and short pulse width of 10^{-12} second. Through high pulse overlapping, it could avoid the thermal damage and create high-quality surface modification. Consequently, such a cold-ablation way greatly improves the performance of the textured material. Therefore, this technology has been widely used for creating different micro/nanostructures on different materials like metals, organic materials, ceramics, and composites for various applications.[79-87] These applications in turn demonstrate its advantages over nano-/milli-second laser microstructuring, including a much-lowered heat load, reduced HAZ, higher energy intensities, rapid heating, and higher average powers. Moreover, it has reduced costs, less system complexity, and better reliability as compared to femtosecond lasers, a much shorter pulse laser.[88] For example, Yu et al. used a 1064 nm picosecond-pulsed laser (10 ps) to form well-structured microgroove (30 μm in width and 1.39-4.03 μm in depth) textures on titanium alloy implants for osteoblast adhesion and proliferation.[89] By optimizing laser processing parameters, the laser power, repetition frequency and scan speed for desired topography quality and detailed dimensions were determined to be about 20 W, 400 kHz, and 1200-2000 mm/s. The promoting function of laser-processing structures to cell adhesion was demonstrated. To mitigate the debris generation and obtain high-quality structure, pulse laser power is usually limited below 0.053 J/cm^2.[90] In view of the relatively lower HAZ,[91] picosecond pulsed laser has also been employed for surface micro/nanostructuring of sensing materials to improve the sensing capability. As reported, the performance of SERS significantly relies on its micro/nanostructured substrate. Aiming at this goal, Byram et al. employed liquid-assisted picosecond laser ablation (532 nm, 30 ps, 10-25 mJ) to fabricate Au NPs with diameters of 5-15 nm and NSs of 150-700 nm as SERS platforms (Figure 4a).[92] The resulting NSs could sensitively and selectively detect multiple analytes like rhodamine 6G, methylene blue, crystal violet, and malachite green due to proper and controllable sizes for plasmonic properties. It is demonstrated that the size and shape of NPs/NSs can be tuned controllably via varying the laser parameters such as laser energy, wavelength, pulse width, and pulse shape.[93] Furthermore, the productivity of NPs/NSs

significantly depends on the laser pulse duration. Based on these merits, various liquid-assisted laser-ablated gold or silver NPs have been developed for SERS sensing owing to their ubiquitous plasmonic properties in past years.[94-96] Recently, this technology began to function in the treatment of 2D transition metal dichalcogenide for sensors. With a picosecond pulsed laser thermolysis (1060 nm, 100 ps, 2.52-2.61 J/cm^2), Park et al. synthesized crumpled 2D MoS_2 nanomaterials in a fast, non-vacuum, wafer-scale, and patternable fashion (Figure 4b).[97] The resultant MoS_2-based device not only presented high-performance triboelectric energy harvesting output than other MoS_2-based ones from other techniques, but also showed good triboelectric sensitivity as a self-powered haptic sensor. It is found that the MoS_2-surface morphology and sensing ability can also be easily controlled by adjusting the laser irradiation. To achieve high spatial resolution and surmount the crosstalk problem in pressure sensor arrays at low fabrication cost, picosecond laser processing (355 nm, 2.1-6.8 W) was employed by Li's group to create a sensor array with a high resolution of 0.7 mm from a polymeric multi-layer stack.[98] Low and high laser power were jointly used to generate isolated piezoresistive 3D graphene pixels and form an interconnect pattern to connect individual pixels (Figure 4c). The obtained mapping sensor exhibited a high sensitivity of 1.37 kPa^{-1}, a wide pressure working range of 80 kPa, a fast response time of 20 ms, and good cycle stability. Such a good sensing ability was further demonstrated in tactile pattern recognition and tumor tissue identification. Despite high-performance sensors achieved by picosecond laser, expensive processing equipment and unsatisfactory resolution largely hinders its wide commercial applications. Moreover, it is still a challenge to achieve some micro/nanostructures with high roughness levels or hierarchical architectures on arbitrary surfaces. To surmount this challenge, Kuisat et al. combined different laser micro-/nanostructuring techniques, nanosecond pulse and picosecond pulse (1064 nm, 10 ns or 10 ps, 3.2 J/cm^2 or 100 W), to construct multiscale structures with feature sizes between 800 nm and 21 μm (Figure 4d).[99] The treated Ti64 and Al-Mg-Sc (Scalmalloy) surface exhibited desired patterned roughness across multiple scales for implementing water-/ice-repellent properties. Consequently, with the micro/nanofabrication moving forward, more complex structures with high scales will be achieved by the combination of these micro/nanofabrication or the exploration of new techniques.

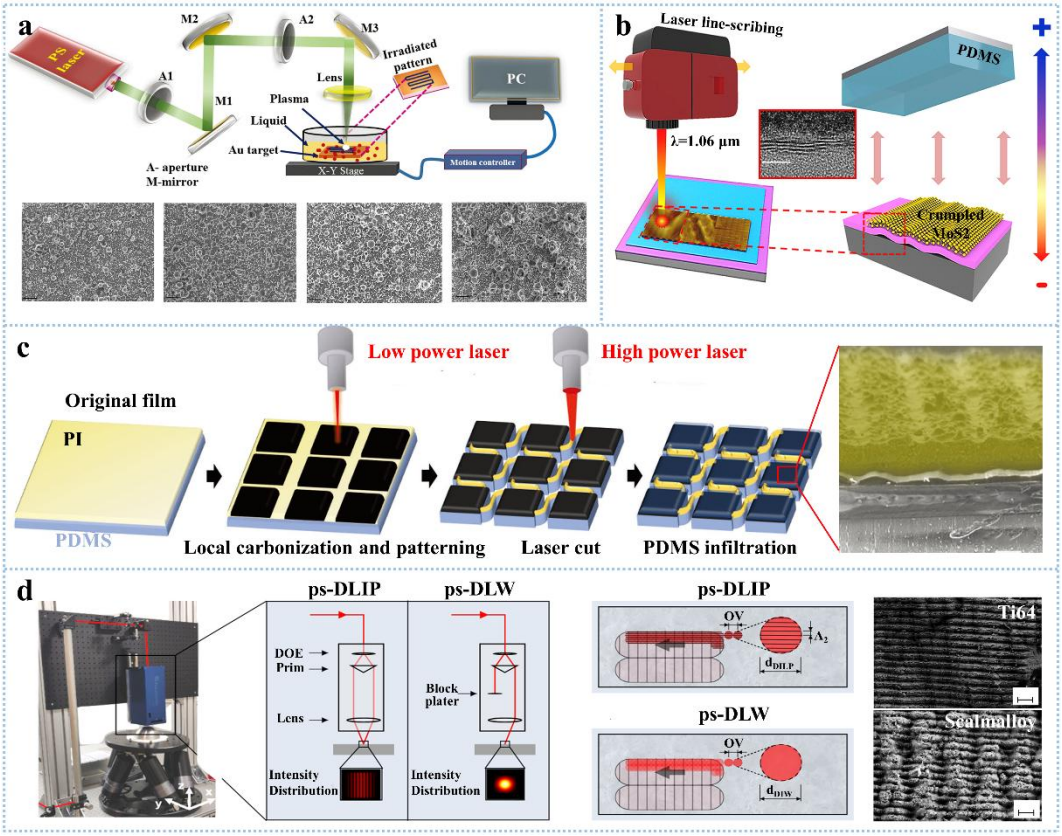

Figure 4. Picosecond laser micro/nanostructuring processing. a) Schematic of the preparation of Au NPs and NSs using a picosecond pulsed laser and the corresponding structures with different laser-textured portions or nanocavities under various pulse energies. Reproduced with permission.[92] Copyright 2019, Royal Society of Chemistry. b) Schematic illustration of laser-directed synthesis of 2D MoS_2 on the SiO_2/Si wafer and its surface morphology of strain-induced crumpled MoS_2 structure. Reproduced with permission.[97] Copyright 2020, Elsevier. c) Two-step laser manufacturing process of the piezoresistive material array with the serpentine interconnect using a picosecond laser, showing the maintained surface roughness for good sensing responses and unchanged individual pixels during the bending of the sensor array. Reproduced with permission.[98] Copyright 2022, Wiley-VCH. d) Schematic of experimental setups and processes for ps-DLIP and ps-DLW process, showing well-defined patterns with different specific textured characteristics on Ti64 and Scalmalloy. Reproduced with permission.[99] Copyright 2022, the authors, published by Wiley-VCH.

2.4 Femtosecond lasers

As an ultra-short pulse laser, femtosecond lasers have extremely short pulse widths with a duration of only 10^{-15} s compared with other pulsed lasers. Due to extremely short energy absorption and laser relaxation time, this ultrashort pulse brings ultra-strong electric field, extremely high peak power, and low thermal effect on the areas surrounding the focal point. Its machining ability was first demonstrated in 1987 when a fs-pulse (160 fs) UV (308 nm) laser

was used to etch the micron-scale features on PMMA surfaces,[100] also verified by the fabrication of sub-micron holes on silver film surface via a 800 nm femtosecond laser in 1995.[101] Since Davis et al. reported its writing waveguides in glass in 1996,[102] it has been widely explored for micromachining. Once interacting with materials, this laser releases the ultrahigh instantaneous power, then leads to a nonlinear absorption effect that breakthroughs the diffraction limit of optical processing, finally forming micro or nano structures on the surface of targeted materials. Moreover, high local energy density makes it suitable for treating all types of materials to obtain desired complex structures, including soft polymer materials, metals, semiconductors and other materials.[103-108] Together with almost no thermal damage to the non-processed zone of the materials, femtosecond laser machining has become a promising cold processing tool for the precision processing of various structures ranging from microscale, submicron to nanoscale, causing extensive applications in the fields of micro-optics, microfluidics, biomedicine, and so on.[109-113] Until now, a large number of femtosecond-laser fabrication structures or devices have been achieved successfully, among which possible ablation mechanisms have been proposed, involving melting, vaporization, coulomb explosion, phase explosion and separation, fragmentation, and spallation.[114] At the earliest, Vorobyev et al. reviewed the advancement in femtosecond-laser-textured nano/microstructures and their applications.[115] Afterward, a mass of reviews have been summarized to elucidate the progress on this technology from the fabrication, mechanism, applications points of view.[116-118] Remarkably, the nanostructures achieved by this technology greatly improve the performance of the treated materials for sensing applications due to common nanoscale effect like surface effect, small-size effect, and quantum tunnelling effect. To realize high-throughput and low-cost fabrication of optical nanostructures for biosensors, Kuznetsov combined femtosecond-laser-induced transfer (800 nm, 30 fs, 0.06 J/cm^2) with nanosphere lithography to fabricate microstructures consisting of hexagonal arrays of spherical Au NPs of around 40 nm partially embedded into a polymeric substrate.[119] The resultant easy-to-use sensors presented a high sensitivity of 350 nm/RIU and a figure of merit of 21.5 in the visible spectral range because of the refractive index changes of local environment caused by diffractive coupling of localized surface plasmons of the laser-machining nanoparticles in the arrays. Using the same laser processing approach (800 nm, 150 fs, 20-25 nJ), Buividas et al. constructed textured dielectric surfaces that are nanoroughness with feature sizes of 20-30 nm as SERS substrates with even

higher sensitivity and reproducibility compared to the lithographically made commercial substrates.[120] Laser-textured ripples coated by gold nanoparticles showed up to 15 times higher SERS signal with a 2 times better signal uniformity as compared to Klarite commercial substrate (Figure 5b). To completely concentrate the target molecules within a sensitive area and enhance SERS detection sensitivity, Cheng et al. employed femtosecond laser (800 nm, 104 fs, 5 mW) to prepare the hierarchically ordered microcrater array with a diameter of about 4-14 μm coated with plasmonic nanoparticle clusters as a surface-enhanced Raman substrate (Figure 5c).[121] The co-exist of hierarchical micro-/nanostructures and satisfactory plasmonic nanostructures enabled the superhydrophobic substrates to show the easily attainable Raman signal EF of ~4.82×10^8 and good uniformity. Utilizing a microsphere-assisted strategy, Zhang et al. integrated it with femtosecond laser double-pulse fabrication (800 nm, 35 fs, 1.98-2.69 J/cm^2) to produce a 3D hexagonal ring-like array under different picosecond ranged pulse delay, that fails to be realized by single 2D laser micro/nanohole patterning method.[106] The fused silica substrate covered with a layer of PS microspheres with a diameter of 1 μm was firstly ablated by femtosecond laser and then etched with KOH. Because of the metal-like mask screening effect of PS microspheres and the use of double pulses, a uniform hexagonal ring-like array was constructed on the silica with a controlled thickness (Figure 5d). This hexagonal ring-like array was not obtained through traditional single pulse irradiation. Considering the advantages of its high electric field and tunable light polarization directions in nanomaterial fabrication, femtosecond laser processing has been used to fabricate quantum dots and 1D nanoparticles for sensing applications.[122-125] Ye et al. irradiated sub-stoichiometric molybdenum oxide nanosheets from MoS_2 powders suspended in ethanol/water with a femtosecond laser (800 nm, 35 fs, 2 W) (Figure 5e).[126] Due to the Coulomb explosion, photoexfoliation, and oxidation of MoS_2 powders caused by femtosecond laser, the H_XMoO_3 with an average size of 30 nm was formed, accompanied by enough oxygen vacancies for LSPR. Although great efforts made and tremendous achievement were obtained, femtosecond laser processing still has some drawbacks to limit its widely practical applications. Due to its point-by-point scanning processing characteristics, the fabrication process of large-area samples usually takes a long time. Moreover, physical mechanism of femtosecond laser processing is still unclear. The short pulse ablation mechanism needs further understanding and to be explored. Compared to picosecond laser and even long-pulse laser, it could fabricate higher-

quality surface features due to the reduced HAZ, but high and uncompetitive cost of the processing facility is also a critical concern.

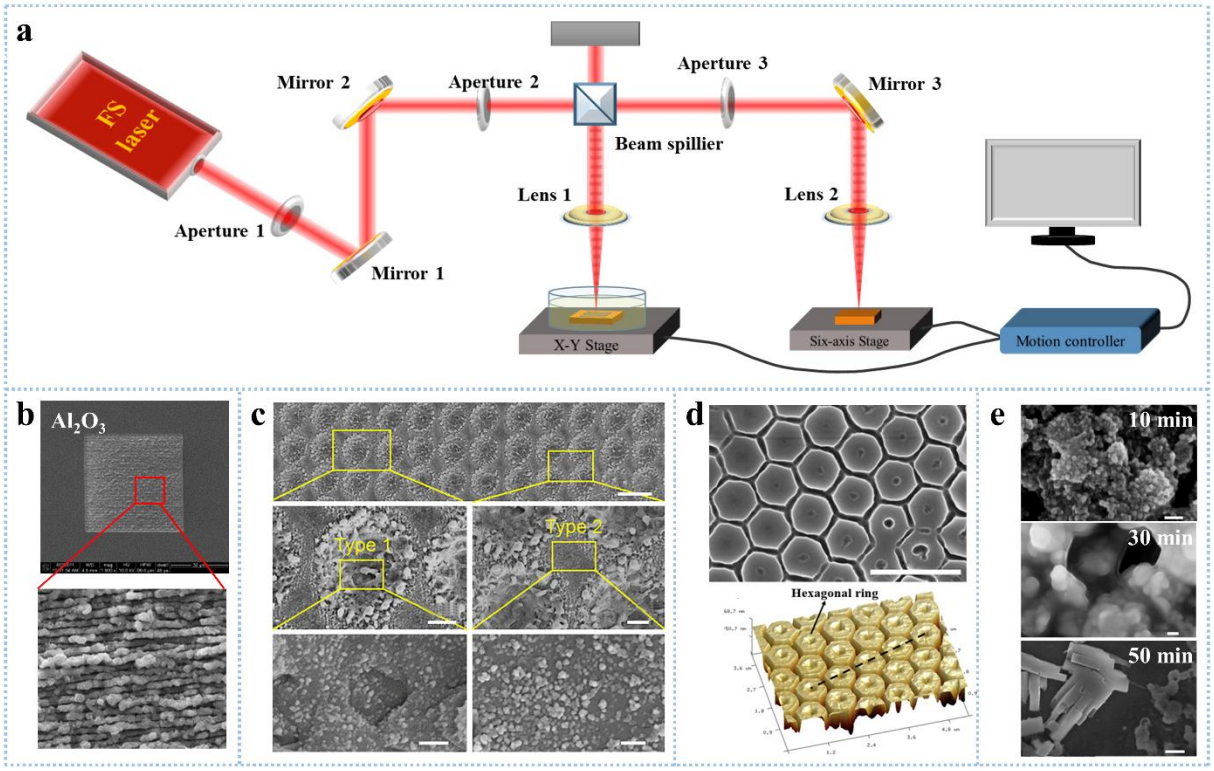

Figure 5. Femtosecond laser micro/nanostructuring processing. a) Schematic illustration of femtosecond laser micro/nanofabrication under different conditions. b) Micro-ripples in 50×50 μm squares irradiated by a linearly polarized laser with the pulse duration of 150 fs. Reproduced with permission.[120] Copyright 2022, Wiley-VCH. c) Highly uniform circular microcrater array fabricated by a femtosecond laser with a pulse width of 104 fs. Reproduced with permission.[121] Copyright 2020, Elsevier. d) Hexagonal ring-like nanostructure array irradiated by a femtosecond laser with a pulse duration of 35 fs. Reproduced with permission.[106] Copyright 2021, Elsevier. e) Two-dimensional plasmonic MoS_2 nanomaterials treated by a near-infrared femtosecond laser with a pulse duration of 35 fs at 2 W for 10, 30, and 50 min in 80% ethanol. Reproduced with permission.[126] Copyright 2021, American Chemical Society.

2.5 Others

Except for the use of the above laser for direct ablation, other types of lasers were also used to create micro or nano structures. As stated, the laser produces high local heating temperature up to 2500 °C, which easily breaks C-O, C=O, or C-N bonds of the substrate materials.[127,128] When these broken aromatic fragments rearrange to form graphitic carbon structures, the produced gaseous products around the sample show transient reducing features and then reduce metal ions to produce metal particles,[129,130] thereby forming the laser-induced treatment

strategy. Compared with the conventional high-temperature annealing method, the laser-induced processing avoids particle aggregation and generates a high yield.[131] Since Tour et al. used the laser to treat the wood, cloth, food, and paper at ambient conditions to produce highly conductive porous graphene,[132] laser-induced technology has attracted considerable attention due to facile synthesis and outstanding electrical, thermal, and mechanical properties. For example, the laser-induced processing could obtain graphene with a porous and high-defect nature. Such a texturing graphene greatly improves heterogeneous charge transport during electrochemical sensing, consequently improving the sensitivity.[133] Lin et al. produced porous graphene films with 3D networks with a CO_2 IR microsecond laser (1060 nm, 14 μs, 3.6 W) to irradiate commercial polymer films (Figure 6a).[134] The resulting LIG exhibited high electrical conductivity as well as porous structures with a surface area of 340m^2/g by BET and pore sizes of below 9 nm. Using similar laser-induced/-patterned irradiating treatment (10.6 μm, 5.0-6.7 W), Yan et al. developed a flexible high-resolution TSA on a PI film for self-powered real-time tactile sensing (Figure 6b).[135] The TSA platform achieved real-time visualization of multipoint touch, sliding, and tracking motion trajectory, exhibiting excellent durability and synchronicity. When Kulyk et al. used a 355 nm diode-pumped Nd:YVO_4 pulsed laser to irradiate paper, paper-based humidity and temperature sensors were obtained.[136] The presence of laser-induced porous conductive networks enabled the relative humidity and temperature sensors to exhibit high sensitivities of up to 1.3×10^{-3} $\%RH^{-1}$ and -2.8×10^{-3} $°C^{-1}$, respectively. These results all demonstrated that laser patterning of the materials is a promising solution to directly synthesizing sensing materials for on-chip applications. Carbon materials patterned by this laser-induced technology exhibit high surface areas and high binding affinities to a broad palette of compounds when as sensor platforms.[137] The electronic and chemical modifications of these laser-induced carbon networks facilitate to achieve a higher sensitivity for certain analytes like metal carbides and inorganic salts.[138] Wang et al. employed a CO_2 laser (10.6 μm, 0.97-1.37 W) to treat the films of pre-carbonized organic nanoparticles on the PET for resistive gas-sensing applications (Figure 6c).[139] When impregnating MoC_{1-x} nanoparticles by adding ammonium heptamolybdate into the precursor film, the resulting doping sensitive nano-grain boundaries and high surface area of 433 m^2/g resulted in an improvement of VOC sensing response (-3.7% for 1250 ppm acetone or -0.8% for 900 ppm toluene) at room temperature. Johnson et al. utilized a scalable direct-write laser fabrication to convert PI into LIG with a

groove-like morphology and numerous pores ranging from 2-5 μm for electrochemical detection of neonicotinoid (Figure 6d).[140] The resultant graphene-based sensors could selectively monitor four major neonicotinoids with low detection limits and a rapid response time. The above results all demonstrated that the laser-induced/-patterned structures could boost the sensing ability of the treated substrate. With the innovation of the laser, new laser-texturing technology will emerge gradually for the fabrication of micro/nanomaterials towards various sensing scenarios.

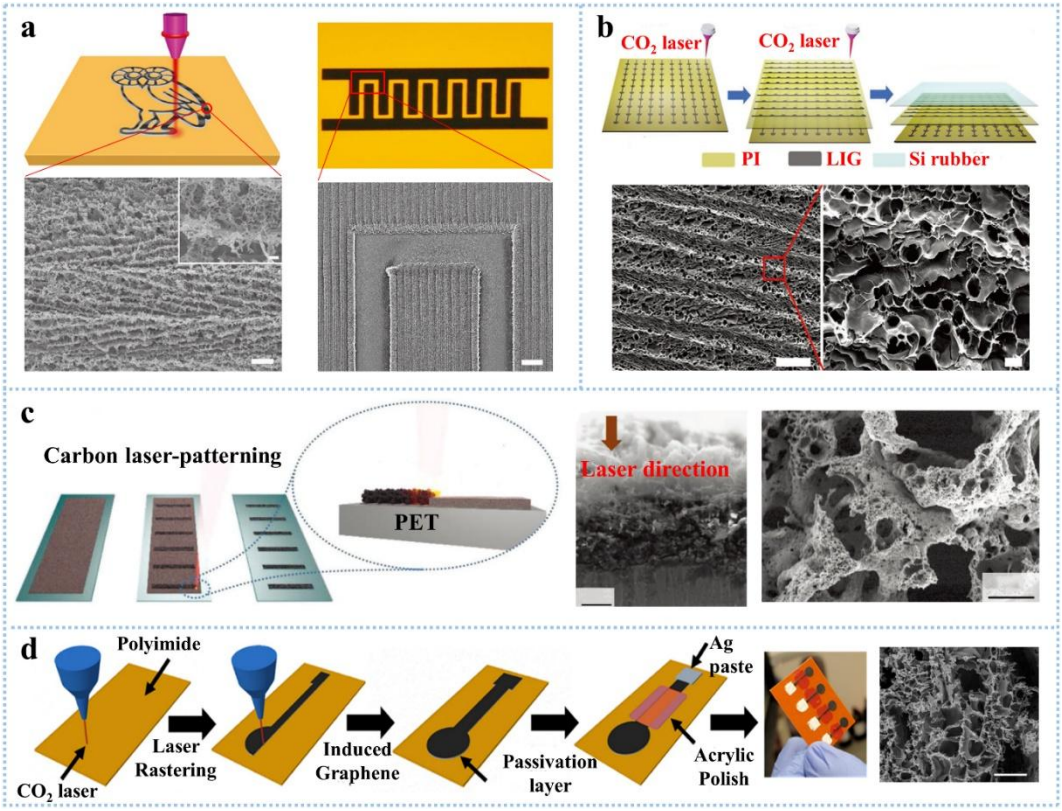

Figure 6. Micro/nanostructuring processing with other lasers. a) The synthesis illustration and the obtained structures of LIG patterns and electrodes from commercial PI films using a CO_2 microsecond laser at a power of 3.6W. Reproduced with permission.[134] Copyright 2014, the authors, published by Nature Publishing Group. b) Fabrication schematic of LIG composed of porous graphene nanosheets with ultrathin randomly stacked reticular structures for a flexible high-resolution triboelectric sensing array. Reproduced with permission.[135] Copyright 2021, Wiley-VCH. c) The fabrication schematic and microstructures of laser-patterning nitrogen-doped carbon (LP-NC) with a porous morphology on the PET for VOC sensing at room temperature. Reproduced with permission.[139] Copyright 2021, the authors, published by Wiley-VCH. d) The synthesis illustration and microstructures of LIG electrode using a CO_2 laser scribing on bare PI. Reproduced with permission.[140] Copyright 2021, American Chemical Society.

3. Laser-textured micro/nanostructures for sensing applications

Based on these flexible laser processing technologies, various functional structures and surfaces have been achieved, exhibiting outstanding sensing ability towards a wide range of analytes including chemicals, mechanical force, and biomolecules. As a partial or whole component, laser-textured micro/nanostructures play a vital role in a variety of chemical sensors, mechanical sensors, electrochemical sensors, and biosensors. To better understand the positive contribution of laser processing to sensing ability, the sensing mechanisms are first discussed briefly below, then three typical groups of sensing applications built on different sensing targets will be elucidated at length in this section, including chemical sensing, physical sensing, and biosensing.

3.1 Sensing mechanisms

It is widely reported that sensor is a conversion device of physical, chemical, biological and other signals collected into easily identifiable electrical or optical signals. Based on this signal conversion, the common sensing mechanisms, including piezoresistivity, piezoelectricity, photoelectricity, chemiresistors, capacitance, electrochemical reaction, SERE, and their combinations (Figure 7), is also suitable for understanding the interfacial and intrinsic behaviors of laser micro/nanostructuring sensors upon adsorbing or capturing different analytes.[20, 22, 141-144] When these laser-processing micro/nanostructures are exposed to external stimulus, the adsorption of analytes or the exertion of actions will trigger the changes of capacitance, resistance, current, and Raman signal of these micro/nanostructures due to the change of surface carriers, chemical bonds, and local structures. Importantly, the presence of micro/nanostructures increases the reaction active sites and improves reaction rate, thereby amplifying the signals and finally enhancing the sensitivity.

Inspired by a capacitor, when assembling laser-texturing dielectric materials and conductive materials together, the resulting device shows changing capacitance upon external stimulus. To increase capacitance variation, a wide range of complex structures have been proposed, such as microscale pyramids, microporous structures, micropillar arrays, and rough interfaces constructed on dielectric materials and conductive materials, which are introduced easily by laser micro/nanostructuring techniques. Through controlling these microstructures, the sensitivity based on capacitance is enhanced greatly.

Since the discovery of piezoelectric effect, it has been used commercially for self-powering devices. Generally, the piezoelectric materials such as PVDF, PZT, and ZnO are directly used

or treated via micro/nanostructuring strategies to produce charge and voltage under pressure.[145,146] Due to the advantage of converting mechanical forces into electrical signals, these materials exhibit good detection behavior to dynamic pressure. The emergence of laser processing technology enables piezoelectric materials to be micro/nanostructured sensor for detecting external forces more sensitively. Similar to piezoelectric sensor, piezoresistive sensor functions through the piezoresistive effect, whose electrical resistivity changes when mechanical strain is applied. Based on this conversion of an external stimulus into resistance change, piezoresistive sensing has been extensively used due to relatively simple structural design, facile readout system, wide detection range, and good durability.[147,148] Through laser texturing design of piezoresistive materials, its contact resistance changes rapidly under external pressure.

Apart from piezoresistive mechanism, another mechanism based on resistance changes is chemiresistive effect, which is a conventional mechanism depending on charge transfer occurring between substrates with electron donating or accepting behaviors and adsorbed molecules, finally changing the substrate resistance.[149] This mechanism is also used to laser textured micro/nanostructures for sensing various chemicals. With the development of sensing technology, electrochemical methods are employed for sensors. Chemical groups (e.g., hydroxyl, carboxyl, and epoxy groups) on the surface of laser micro/nanostructured substrate can act as chemical handles for grafting functional molecules (such as proteins, carbohydrates, and polymers) through covalent bonds.[150] When applying the constant potential or current, chemical groups on the surface of laser-textured substrate make its outputting current or voltage change originated from its affinities to functional molecules. The combination of laser micro/nanostructuring and chemical functionalization further improves the electrochemical sensing performance.

Except for the direct conversion of the above mechanical or chemical stimuli into electrical signals, there is another kind of well-accepted conversion through the electrochemical reaction. This process produces electrical signals like potential or current because of the potential changes triggered by the redox reaction between the target analyte and the recognition layer with the assistance of certain solution. It commonly requires a reference electrode, a counter electrode, and a work electrode where the redox reaction happens. These electrodes function together to convert the responsive information to qualitative and quantitative electrical signals,

thus acting as the well-known sensors for detecting various analytes. Owing to high sensitivity, long-term reliability, high accuracy, rapidity, low cost and easy miniaturization, such sensors based redox mechanism have been extensively explored and summarized.[151] Because the electrode interface is the very site that absorbs targeted molecules and generates redox reaction, thereby playing a vital role in the sensing performance. When laser micro/nanostructing electrode interfaces, the surface morphology and architecture of the electrode could be tailored, thus greatly enhancing not only the electrical conductivity but also the surface area. Both two factors would accelerate the interface redox, finally improving the sensing performance, similar to the enhanced effect in other sensing mechanism when laser micro/nanostructuring is utilized.

Except for the electrical signal produced, optical signals have also been employed in sensors. SERS has been emerging as a highly sensitive molecular analysis technique for trace detection based on SERE due to its highly sensitive, non-destructive and fingerprinting capability. Based on fingerprint identification, it can realize fast and non-destructive identification of the component of analytes by detecting the information of molecular bonds.[152] As demonstrated, the preparation of SERE substrates plays an extremely important role in the development of SERS technology and the application of SERS detection. In view of localized field enhancement from LSPR of metal particles, the construction of micro/nanostructures on the SERE substrate could enhance the Raman signal reflecting vibrational and rotational modes of the analyte molecules. Moreover, this enhancement is determined by the gap and feature size of the metal micro/nanostructures. When combining this signal improvement with SPR based on resonant frequency shift or intensity modulation induced by the refractive index change of the environment or chemical charge transfer, the SERS detection is also improved drastically. For the merits of laser processing in micro/nanostructures or even nanomaterials, laser micro/nanostructuring materials have been extensively studied for a wide range of SERS applications.[153,154] In conclusion, the existing sensing mechanism has been widely used to elucidate and design laser processing micro/nanostructures for sensing applications.

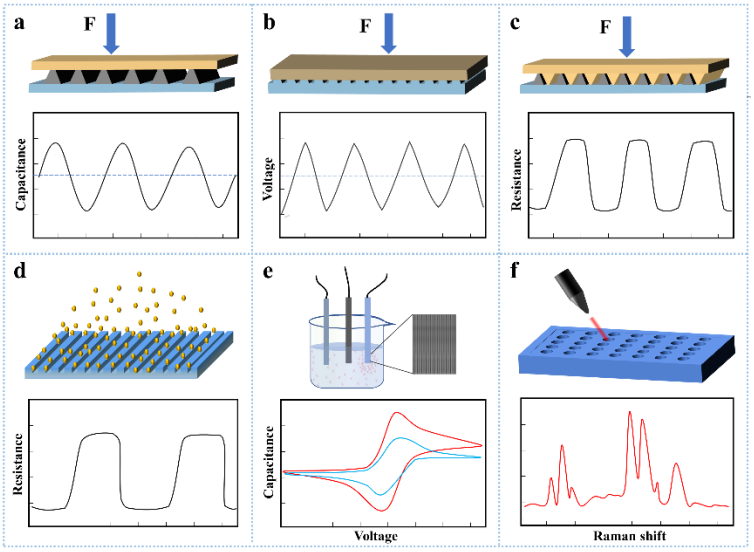

Figure 7. Various sensing mechanisms usually used for laser micro/nanostructuring sensors. a) Capacitance changes under external force. b) Piezoelectric effect. c) Piezoresistive effect. d) Chemiresistive effect. e) Electrochemical reaction. f) Surface enhanced Raman effect.

3.2 Chemical sensing

In consideration of food safety, green environment, and public health, there are great demands on sensing various contaminants in drinking water and air of the surroundings we live. On the basis of the aforementioned working mechanism of the reported sensors, the variation in electrical signals including resistance, capacitance, voltage, current, and charge transfer resistance induced by these external stimuli are detected for chemical sensing (Table 2). To improve the sensitivity and simplify the fabrication of the sensor, laser micro/nanostructuring sensors have been explored widely for various applications in the fields of agriculture, aquaculture, and environment.[155-157] Lu et al. utilized a focused diode laser beam (532 nm, 20-140 mW) to modify the surface property of large area MoS_2 films. The obtained complex laser-patterned films could be acted as synthetic templates for the selective self-assembly of Au NPs by laser-induced active nucleation sites.[158] Through varying laser powers and reaction time, the functional properties of the resulting laser micro/nanostructuring hybrid materials were controlled as superior SERS substrates for the detection of aromatic organic molecules. Owing to the synergistic effect of the high-efficient adsorption of these molecules onto laser-patterned MoS_2 and the strong coupling of the self-assembled Au NPs to the Raman signal, the laser micro/nanostructuring hybrids showed strong Raman signal enhancement for R6G, R101, and MB, presenting sensitive detection ability with the LOD of as low as 1×10^{-9} m. In another example to achieve broad plasmonic response and high enhancement characteristics of SERS

and SEPL towards sensing application, Kuchmizhak et al. utilized single-pulse femtosecond laser (400 nm, 200 fs, 1.2-8.4 J/cm^2) to irradiate silver films for the construction of spallative craters composed of densely packed irregular arrays of nanotips with curvature radii of 10-100 nm.[159] This laser-structured silver films illustrated the strongly enhanced Raman scattering with the averaged SERS EF of 2×10^6, showing good sensing capabilities due to the corresponding local-field enhancement mechanisms originated from the presence of nanotexture and separate individual submicron elements (Figure 8a). Recently, to achieve large-area, low-cost SERS substrates, Erkızan et al. utilized a direct laser writing technique (1032 or 1550 nm, 370 or 450 fs, 1.2 μJ or 2600 J/cm^2) to produce periodic nanostructured surfaces with LSFL and HSFL patterns as well as periodicities of 290 and 890 nm. After the deposition of a thin noble metal layer of 50-70 nm, the SERS substrates are found to be capable of detecting a Raman analyte down to 10^{-11} m. Both LSFL and HSFL surfaces with 70 nm thick Ag exhibited the strongest SERS with Raman EFs as high as 10^9.[160] Considering the importance of a hybrid nanostructure for improving the sensing performance, Zhang et al. incorporated Au NPs to decorate ZnO nanospheres by laser irradiation-induced heating-melting-evaporating processes (355 nm, 40 mJ) (Figure 8b).[161] The as-formed Au-ZnO nanospheres with an average size of 40-65 nm showed significantly enhanced gas sensing properties compared with those of pure ZnO nanospheres, with the response values of 252 to100 ppm ethanol (Figure 8b). Using similar femtosecond-pulsed laser ablation in liquid technique (800 nm, 50fs, 300 μJ), Bharati et al. fabricated Ag@Au and Cu@Au alloy nanoparticles in $HAuCl_4$ solution.[162] The fabricated composite NPs with tens of nanometers could sense explosive molecules such as 2,4,6-trinitrophenol, 2,4-dinitrotoluene, and MB, with the LOD as low as few nano-/pico-grams.

Table 2. Performance, structure desing, and applications of chemical sensors prepared by various laser micro/nanostructuring strategies.

Materials	Mechanism	Laser parameters	Sensitivity and response	Micro/nanostructures	Targets	Applications	Ref
TiO_2, $AuCl_4^-$	Resistance	ms laser (1064 nm, 1 ms, 5 kW)	LOD: 5 ppm (NH_3) 40 ppm (acetaldehyde) 50 ppm (benzene) 28 s, 59 s, 39 s	Au@TiO_2 NSs 10.8-14.4@106 nm	NH_3 Acetaldehyde Benzene	Gas sensors	60
GO	Resistance	ns Nd:YAG laser (10 ns, 0.1-0.3W)	2 s (11-95% RH)	Hierarchical micro-NSs	H_2O	Graphene-based microdevices	74
Au target	SERE	ps laser (532, 30 ps, 10-25 mJ)	LOD: 5 μM	Au NPs (5-15 nm) Au NSs (150-700 nm)	Dye, Explosive mixtures	SERS multiplex sensor	92
Bulk Au	SERE	fs laser	EFs: 10^3, 10^4, 10^5, 10^6	Au NPs/NSs with	AN	SERS-based	94

target		(800, 50 fs, 0.2-0.5 mJ)	LOD: 10^{-5}, 10^{-6}, 10^{-7}, 10^{-8} M	nanopores, nanorims, nanodroplets, nanoprotrusions	PA Rh6G MB	sensor	
Au flake	SERE	ns Nd:YAG laser (1064 nm, 10 ns, 90 mJ)	LOD: 10^{-13} M	Chain-like Au NPs	R6G	SERS-based sensor	95
Au/Ag targets	SERE	fs laser (1045 nm, 457 fs, 25-80 mW)	LOD: 10^{-10} M	NPs with different sizes	MB	SERS-based sensor	96
Glass, Cu-Ag films	SERE	fs laser (1045 nm, 457 fs, 25-80 mW)	LOD: 10 ppb	Periodic metal NSs (250 nm periodicity) in 3D microchannels	Cd^{2+}	Microfluidic SERS platforms	110
Au	LSPR	fs laser (800 nm, 30 fs, 0.06 J/cm^2)	365 nm/RIU Figure of merit: 21.5	Periodic arrays of spherical 40 nm Au NPs	Glycerin	Optical sensor	119
Filter paper	Resistance	Nd:YVO_4 pulsed laser (355 nm, 3 W)	LOD: 1.3×10^{-3}%RH^{-1}	Porous fibrous structure	H_2O	Paper-based sensor	136
CNFA NaI $(NH_4)_2MoO_4$	Chemo-resistive	CO_2 laser (10.6 μm, 0.97-1.37 W)	$\Delta R/R_0$ = -3.7% (acetone) -0.8% (toluene)	Foamy carbon network with macro and mesopores (433 m^2/g)	VOC	Chemical sensors, selective sensor arrays	139
PI film	ECR	CO_2 laser (5.25 W)	LOD: 338-823 nM ~10 s	Porous groove-like morphology (pores: 2-5 μm)	Neonicotinoid	Electrochemical sensor	140
Wood	SERE	CO_2 laser	LOD: ~ 0.1% 0.2 s	3D microfluidic channel	O_2	Microfluidic sensor, plasmonic-based sensing	156
PLGA	SERE	Raman laser (785 nm, 0.018-0.064 mW/μm^2)	EF: 3.38 × 10^6	Regular cluster arrays from hexagonally packed nanospheres	MBA	Immune assays	157
$AuCl_3$ solution, MoS_2 film	SERE	Diode laser (532 nm, 20-140 mW)	EF: 307.9 (R6G) 218.5 (MB) 1843.5 (R101) LOD: 10×10^{-9} M (R6G), 1×10^{-9} M (MB, R101)	Au NPs decorated micropatterns	R6G MB R101	Biomolecule detection, biomedicine, pesticides detection	158
Ag films	SERS, SEPL	fs laser (400 nm, 200 fs, 1.2-8.4 J/cm^2)	EF: 40 (SEPL) 2×10^6 (SERS)	Spallative craters with irregular nanotip arrays (Radii: 10-100 nm)	R6G	Chemo/biosensing	159
Ag films	SERE	fs laser (1032 or1550 nm, 370 or 450 fs, 1.2 μJ or 2600 J/cm^2)	EF: 1.9 × 10^9 (HSFL) 1.6 × 10^9 (LSFL) LOD: 10^{-11} M (HSFL) 10^{-10} M (LSFL)	Periodic nanostructured surfaces with LSFL and HSFL patterns	Crystal violet	Trace analyte detection	160
ZnO, $HAuCl_4$	Chemo-resistive	Pulsed laser (355 nm, 40 mJ)	EF: 252 (100 ppm)	Hierarchical nanospheres (40-65 nm)	Ethanol	Gas sensing materials	161
Ag/Cu target, $HAuCl_4$	SERE	fs laser (800 nm, 50 fs, 300 μJ)	~10^4 (PA), ~10^5 (DNT), ~10^7 (MB)	Ag@Au, Cu@Au alloy NPs with tens of nm	TNP DNT MB	On-site & field-based detection	162
PI sheets，	ECR	CO_2 laser	1.08 g/L(5-10 g/L Cd^{2+})	3D porous stacked sheet	Cd^{2+}	Heavy metal sensor	163

PANI, PVP		(5-6.2 W)	0.16 g/L(10-380 g/L Pb^{2+})	structures	Pb^{2+}		
rGO/GO/rGO	ECR	Blue-violet CW semiconductor laser, (405 nm, 28.7 mW)	LOD: 6.3%RH	Porous layered structure (thickness: 3 μm)	H_2O	Humidity sensors	164
Paperboard	Chemo-resistive	CO_2 laser (8.4-25.5 W)	LOD: 0.33% (0.11-40.6%)	Interdigitated array with porous carbon material	NH_3	Gas sensors, fuel industry	165
PI film	ECR	CO_2 laser (2.25-5.25 W)	60.87 mV/dec (K^+) -57.87 mV/dec (NO_3^-) 51.66 mV/dec (NH_4^+) LOD: $10^{-5.01}$ M, $10^{-5.07}$ M, $10^{-4.89}$ M, 15.4 pM	Hierarchical porous graphene structures with different DPI	K^+ NO_3^- NH_4^+ Pesticide	POCT, environmental monitoring	166
PI sheets	ECR	CO_2 laser UV (355 nm, 1 μs, 0.25 W) IR (10.6 μm, 9.0 W)	93 μA/μm cm^2 (0.5-3×10^{-6} IR) 58 μA/μm cm^2 (0.5-4×10^{-6} UV)	3D-like arrangement of interconnected flakes with various porosities	DA	Carbon-based sensors	167
Cu foil	Terahertz	fs laser (780 nm, 100 fs, 1.6-2.2 W)	$\Delta T/T$ = 0.1 mg/L (0-10000 mg/L)	Periodic metallic-hole-arrays-complementary asymmetry split rings	Fruit acids	In situ analysis, food products	168
AuNPs PI foil	ECR	CO_2 laser	LOD: 1.2 ng/mL (3-4000 ng/mL)	3D foam-like porous structure	OPs	Higher-performance POCT device	169
Ag/Au, Si	SEFE	fs Yb:KGW laser (515 nm, 200 fs, 0.1 or 0.16 J/cm^2)	LOD: 0.15 nM (0.1 μM-0.1 mM)	Periodic surface structures	Hg^{2+}	Plasmon-related applications	170

To overcome the narrow detection ranges of graphene-based sensors, Lin et al. utilized the laser-engraving technique (CO_2 laser, 5-6.2 W) to fabricate a high-quality 3D nitrogen-doped porous graphene-based sensor.[163] Based on the unique electrochemical properties and the 3D porous structure framework with large electrochemical active surface areas, the graphene-based sensor could simultaneously determine Cd(II) and Pb(II), presenting quite wide linear ranges (5-380 g/L for Cd(II) and 0.5-380 μg/L for Pb(II)) and low LOD (nearly 3 times and 60 times less than the guideline values of the drinking water presented by the World Health Organization). This improvement was also demonstrated by detecting tests in actual water samples. Utilizing a femtosecond-laser-assisted wet etching (1045 nm, 457 fs, 25-80 mW), Bai et al. prepared periodic metal nanostructures with a periodicity of 250 nm inside 3D glass microfluidic channels. [110] The resulting SERS microfluidic chip could achieve the real-time SERS detection of Cd(II) ions at concentrations as low as 10 ppb (Figure 8c). To achieve a fast and highly sensitive humidity sensor, Cai et al. constructed a patterned rGO/GO/rGO layered structure of 3 μm in thickness by a facile blue-violet CW laser direct writing method (405 nm, 28.7 mW), which is capable of sensing humidity on a smartphone for portable electronics.[164] Different

from conventional resistance, impedance, or capacitance mechanism, this sensor detected humidity based on the output voltage change. It exhibited a dramatically enhanced sensitivity by about 45 times and an obvious response to the relative humidity of 6.3-100%. Outstanding cycling stability, flexibility, and long-term stability (>1 year), as well as good reproducibility enabled the actual humidity sensing by easy connection to an iPhone (Figure 8d). To monitor ammonia (NH_3) in air with a common paper, Reynolds et al. fabricated a paper derived NH_3 gas sensor using a direct laser scribing method (CO_2 laser, 8.4-25.5 W).[165] Utilizing the dependence of the sensor resistance on the NH_3 concentration, the formed carbon-based interdigitated array composed of porous carbon materials on papers presented good selectivity toward ammonia and excellent sensitivity. Recently, to create both the microfluidics and electrochemical cells in a scalable fashion for sensors, a CO_2 laser-induced technique (2.25-5.25W) was utilized to form laser-induced patterned graphene with different electrical conductivity, surface morphology with different DPI, and surface wettability.[166] The obtained ion selective electrodes could both monitor potassium (K^+), nitrate (NO_3^-), ammonium (NH_4^+) and sensing organophosphate pesticide (parathion), showing near-Nernstian sensitivities and lower LOD (Figure 8e). Utilizing a similar laser-induced strategy for graphene, Santos et al. produced LIG electrodes composed of 3D-like arrangement of interconnected flakes with different scaled pores via CO_2 UV laser (355 nm, 1 μs, 0.25 W) and infrared laser (10.6 μm, 9.0 W) irradiation on PI sheets, which exhibited good selectivity and extreme sensitivities for DA even if at physiologically relevant DA concentrations (Figure 8f).[167] Benefiting from the advantages of timesaving, cost-effective, and high-throughput features, Zhou et al. used laser direct writing technology (780 nm, 100 fs, 1.6-2.2 W) to prepare free-standing THz metamaterials to rapidly detect organic acids for determining fruit taste.[168] Through optimizing fabrication parameters, the THz metamaterials could be optimized to distinguish fruit acid with a concentration of 0.1 mg L^{-1} quickly and simply. This strategy demonstrated huge potential for rapid *in situ* analysis of flavor components in food products. To further improve the sensor with portable, quantitative, and user-friendly features for guaranteeing food safety, Liu et al. used integrated LIG electrode on a PI film and MnO_2 nanosheets loaded on the paper for POCT of OPs residues.[169] Relying on acetylcholinesterase AChE-catalyzed hydrolytic product-triggered disintegration of MnO_2 nanosheets for releasing assistant DNA to initiate nicking enzyme-aided recycling amplification, the proposed sensor exhibited a satisfactory linear range

from 3 to 4000 ng/mL and LOD down to 1.2 ng/mL for OPs assay, also supported by the evaluation of the residual level of pesticides in the vegetables. In a word, the utilization of laser processing micro/nanostructures for chemical sensing has made great progress so far, bringing us a potential way to improve the sensing performance. However, with the demand on the multiplex detection rising in recent year due to complex surroundings, new challenges emerge in multiplex analyses for practical implementation, offering a new requirement for advanced structure designs.

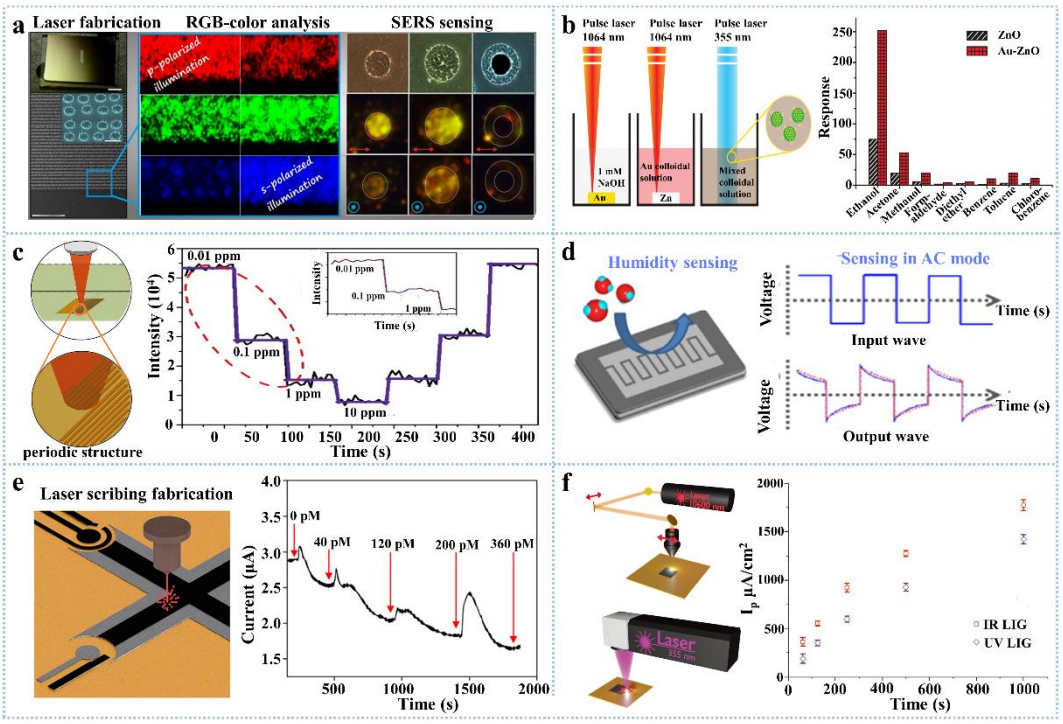

Figure 8. Chemical sensing ability of laser micro/nanostructuring materials. a) Large-scale nanotextured Ag film produced by a femtosecond laser shows more enhanced SEPL and SERS response for R6G marker, supported by Red-Green-Blue (RGB) color analysis of their polarization-resolved dark-field scattering images. Reproduced with permission.[159] Copyright 2016, American Chemical Society. b) The synthesis schematic of Au-ZnO nanospheres showing excellent selectivity when successive exposure to 100 ppm of various gases compared to pure ZnO nanospheres. Reproduced with permission.[161] Copyright 2016, Royal Society of Chemistry. c) Femtosecond-laser-induced periodic surface structures for the fabrication of a 3D microfluidic SERS chip showing the real-time SERS sensing of Cd^{2+} solutions with concentrations of 0.01, 0.1, 1, and 10 ppm. Reproduced with permission.[110] Copyright 2018, Wiley-VCH. d) A high-performance all-graphene humidity sensor prepared by laser direct writing, showing good alternative-current mode sensing. Reproduced with permission.[164] Copyright 2018, American Chemical Society. e) Fabrication schematic of the all-in-one open-microfluidics multiplex sensing platform showing the current *vs* time

response to different concentrations of parathion for pesticide sensing. Reproduced with permission.[166] Copyright 2021, American Chemical Society. f) Schematics of the fabrication of LIG on PI sheets with gantry scan system of the CO_2 laser and galvanometric system of the UV laser. The resultant LIGs show linear responses and extreme sensitivities for DA oxidation. Reproduced with permission.[167] Copyright 2021, Wiley-VCH.

3.3 Physical sensing

Table 3. Performance, structure formation, and applications of physical sensors fabricated by various laser micro/nanostructuring strategies.

Materials	Mechanism	Laser parameters	Sensitivity	Micro/nanostructure	Stability/ response	Applications	Ref
-PEEK	Resistance	ns laser (355 nm, 25 ns, 5.5 W)	GF: 9.198 (0-0.29% strain)	Patterned foamy dense structures	⩾ 800 cycles	Digitalized medical devices, personalized smart orthopedics	87
PDMS, PI	Piezo-resistive	UV laser (355 nm, 6.8 W)	1.37 kPa^{-1} (< 80 kPa)	3D porous G network (Thickness: 22-35 μm)	10000 cycles 20 ms	Flexible pressure sensor arrays, tactile pattern recognition	98
PI	Tribo-electric	CO_2 IR layer (10.6 μm, 100 W/5.0-6.7 W)	0.016 V kPa^{-1} (< 200 kPa)	Porous randomly stacked reticular structure	6000 cycles	Prosthetics, healthcare monitoring, HMI	135
CNT paper	Capacitive	1.06 μm fiber laser	GF: 37 (3% strain)	Pre-crack strip pattern	> 1000 cycles	Wireless strain sensors	171
Si	Piezo-resistive	UV laser	GF: 33 (0-350 ppm)	Rough micro/nano-texturing surface	1000 cycles 8 s	Nano mechanical-sensors	172
PDMS-C composites	Capacitive	CO_2 laser	$\Delta C/C_0$ = 80%	Interdigitated pattern (line widths: < 100 μm, resolution: 1 μm)	> 10^6 cycles	Multifunctional stretchable sensors	173
Silicone elastomer	Capacitive	DPSS laser (355 nm, 0.42 W)	0.38 (0<ε<0.85) 0.90 (ε = 0.85)	Microgroove pattens Roughness: 1.26 μm	1000 cycles 0.146 ms	Human motion monitoring, physiology monitoring, HMI	174
PDMS	Resistance	fs laser (1030 nm, 780 fs, 5.0W)	-1.82 kPa^{-1} (< 2 kPa) LOD: 0.001 kPa	Micro-domes (Height: ~19.5 μm, diameter: ~22.8 μm)	6000 cycles 0.036 s	Pressure sensors, epidermal electronic skin (e-skin)	175
Acrylic mold, PDMS	Capacitive	CO_2 laser (10.6 μm, 11.25 W)	0.221% Pa^{-1} (0-100 Pa) 0.033% Pa^{-1} (0.1-1 kPa) 0.011% Pa^{-1} (1-10 kPa)	Pyramid shaped microstructures	1000 cycles 50 ms	Smart e-skin	176
PDMS, CNT	Piezo-resistive	Laser etching system (405 nm, 1.96 W)	6.417 kPa^{-1} (1.2 to 1.4 MPa) 1.1 kPa^{-1} (<1.2 kPa)	Periodic micropillar of 100 μm in diameter	7000 s 4 ms	Wearable electronics	177
MXene, PET	Piezo-resistive	Cold UV laser	99.5 kPa^{-1} (<1 kPa) 4.0 kPa^{-1} (1-4.5 kPa) LOD: 9 Pa	Fingerprint-like circle arrays with an internal distance of 80 μm	10000 cycles 4 ms	Micro-force sensing, health monitoring, intelligent robotics, HMI	178
PI	Resistance	Nano-pulsed laser (1064 nm, 100 kHz)	0.00142 $°C^{-1}$	3D pattern with porous structure	5000 cycles ≈1 s	Wearable on-skin electronic devices	179

G	Resistance	fs laser (515 nm, 600 fs, 75 W)	GF: 496.7 (10%)	100 μm circle array	100 cycles	Multifunctional sensor, e-skin	180
PI, BP	Resistance	CO_2 IR laser (10.6 μm, 7.2 W)	GF: 2765 (< 19.2%) LOD: 0.023%	3D pattern with porous graphene structure	> 18400 cycles 83.6 ms	E-skin, robotic appendages, health monitoring technologies	181
$HAuCl_4$, GO	Resistance	fs laser (780 nm, 70 fs, 3-7 mW)	GF: 52.5 (0-25.4% strain)	Square-lattice-like microcrack networks from 10-400 nm AuNPs	500 cycles, operation > 1 year	Artificial skin, wearable electronics	182
CNFA ink	Resistance	CO_2 laser (10.6 μm, 60 W)	$\Delta R/R_0$ = -5% (< 60 kPa) -(5-10)% (> 60 kPa)	Sponge-like porous foamy structure	600 cycles	Mechanical sensors	183
PDMS	Piezo-resistive	fs laser (355 nm, 500 fs, 1-8 W)	4.48 kPa^{-1} (0-22 kPa) 0.86 kPa^{-1} (27-65 kPa) LOD: 3 Pa	Hierarchical microstructures of periodical pyramids	>1000 cycles < 7 ms	Medical monitoring Devices, HMI	184
MXene-coated PU	Resistance	N.A.	0.45% deg^{-1} (0-120°) ~15°	3D porous network structure	> 1000 cycles 115 ms	Joint movement monitoring	185
EGaIn LM	Resistance	Laser cutting	0.37 Pa^{-1} (0-6667 kPa) LOD: 1.2 N	Patterned micro-convex dome arrays	> 1000 cycles <0.33 s	High-performance sensors, microfluidic platforms, microanalysis systems	186

Apart from various chemical contaminants, external non-chemical stimuli like force and heat also need to be detected. Especially with the health concept rising, to detect human motion and body conditions poses an urgent demand on physical sensors. Based on the mechanism of piezoresistivity, piezoelectricity, and capacitance, laser micro/nanostructuring materials have been extensively explored for sensing physical stimuli due to improved sensitivity and facile fabrication, as summarized in Table 3. Using focused ion beam and laser engraving technology, Phan et al. fabricated a proof-of-concept nanowire-pressure sensor.[172] The presence of laser-engraving rough Si membrane endowed piezoresistive sensors with significant 3-fold enhancement in the sensitivity under pressure in comparison to the pressure sensors from micro-sized SiC. As demonstrated in previous studies, micro-structured pressure sensors also present broad pressure sensing range, high sensitivity, and rapid response speeds. However, there are some fabrication issues such as failure in high-resolution patterning over large areas faced by conventional lithography as well as complex preparation procedure or uncontrollable morphology confronted by biomaterial-replicating method. To solve them, Araromi et al. patterned PDMS-carbon composite by CO_2 laser ablation and subsequent oxygen plasma activation to produce high-resolution compliant robust sensor electrodes with line widths of below 100 μm. The use of laser technique brings great design flexibility, high resolution (as

low as 1 μm), and easy scalability to large-area arrays. The resultant interdigitated capacitive touch sensors showed high sensitivity and insensitivity to substrate stretching (Figure 9a).[173] Using a rapid surface modification technique based on direct-write laser raster scanning (355 nm DPSS laser, 0.42 W), Atalay et al. created patterned micro-grooved surfaces with a surface roughness of 1.26 μm on pre-strained elastomeric sheets for highly stretchable and soft capacitance-based strain sensors. After sputtering aluminum and silver metal layers, the fabricated electrodes maintained good electrical conductivity up to 250% strain, enabling the resulting sensor to display a linear and repeatable output up to 85% strain (Figure 9b).[174] With a femtosecond laser processing (1030 nm, 780 fs, 5.0W), Gao et al. also developed micro-structured pressure sensors.[175] A series of micro-structures including micro-ridges and micro-domes were constructed on PDMS elastomers for modulating and enhancing the sensitivity of the sensors (Figure 9c). The obtained sensor with laser-textured micro-domes of ~19.5 μm in height and ~22.8 μm in diameter showed better sensitivity (17 times than the one based on traditional long micro-ridges), rapid response/relaxation speeds, and LOD of 0.001 kPa. By virtue of the similar micro-structured PDMS fabrication, Palaniappan et al. developed a set of PDMSs with pyramid shaped micro-structures using a CO_2 laser engraved acrylic mold (10.6 μm, 11.25 W).[176] After attaching the top and bottom Ag electrodes to the smooth side of pyramid-shaped micro-structured PDMSs, a novel capacitive pressure sensor was obtained for touch sensing applications. When the applied pressures range from 0 to 10 kPa, the sensor presented a sensitivity ranging from 0.221% to 0.011% Pa^{-1}, a fast response time of 50 ms, a recovery time of 150 ms, and excellent cycling stability. These excellent characteristics make the sensor efficiently detect pressure generated by various activities such as hand gesture and carotid pulse measurement.

Based on piezoresistive mechanism, traditionally piezoresistive sensors concentrate on the structure design of the sensing materials to tailor the contact resistance for the improvement of sensitivity and working range. To simultaneously integrate a linear working range (over 100 kPa) and a reliable sensitivity into a sensor, Xu et al. engraved silver-coated fabric with a laser as sensor electrodes.[177] This laser-engraved design composed of periodic micropillars with a diameter of 100 μm markedly enhanced the linear working range to a level of 800 kPa (Figure 9d). The obtained sensor still exhibited a high sensitivity of 6.4 kPa^{-1}, a fast response time of only 4 ms, and good durability. Using a cold UV laser, Gao et al. constructed fingerprint-like

circle micro-channeled arrays with the internal distance of 80 μm to etch the micro-channeled structure, finally obtaining a novel microchannel-confined MXene-based flexible piezoresistive sensor.[178] The cold laser manufacturing effectively guaranteed the smoothness and completeness of fingerprint-like microchannels. These fingerprint micro-structured channels together with the accordion-micro-structured MXene leaded to the synergistically confined effect. This effect made the micro-structured sensor have low LOD, high sensitivity, fast response time, and non-attenuating durability over 10 000 cycles, thereby achieving multiple sensing of pressure, sound, and acceleration simultaneously.

As a highly precise, efficient, and eco-friendly processing method, laser processing technique has been used to synthesize carbon materials for various sensors. Gandla et al. used a rapid bench-top nano-pulsed laser for laser-induced carbonization of PI substrates to produce stable and highly linear temperature sensors.[179] The laser-induced carbonized temperature sensor had a temperature coefficient of resistance of 0.00142 $°C^{-1}$ and exhibited linear and stable behavior under various temperatures (Figure 9e), supported by the potential applications such as blowing, finger touching, breathing, and cold-hot water tests. Ye et al. used a femtosecond laser patterning technology (515 nm, 600 fs, 75 W) to produce the imperfect graphene with different types and distributions of defects.[180] The as-obtained graphene displayed remarkable sensing selectivity owing to the dangling bonds and vacancies on the edge of patterns. The final graphene-based sensors with the 100 μm circle, triangle, and hexagon pattern arrays could detect the strain variation, temperature, and gas, as supported by simultaneous detection of body pulse, temperature, and harmful gas on a human body or garment (Figure 9f). Chhetry et al. integrated laser-engraved graphene and black phosphorus on an ultrathin and resilient polystyrene-block-poly(ethylene-ranbutylene)-block-polystyrene substrate as a highly sensitive dual-modal temperature and strain sensor platform.[181] By virtue of this novel design strategy, the hybridized sensor exhibited high thermal index of 8106 K, high strain sensitivity of up to 2765 (>19.2%), ultralow strain resolution of 0.023%, and longer durability above 18400 cycles, offering unique opportunities for robotic appendages and health monitoring technologies. Considering LIG merits, Wan et al. used a milliwatt femtosecond laser (780 nm, 70 fs, 3-7 mW) to simultaneously reduce graphene oxide film mixed with $HAuCl_4$ solution to form a new class of LIG oxide/Au strain sensor.[182] This sensor based on square-lattice-like microcrack networks from 10-400 nm Au NPs showed high sensitivity (GF 52.5), excellent

stretchability (strain up to 25.4%), full-range linear behavior, and excellent stability over 1 year. Laser treatment resulted in the improved strain sensing performance due to the contribution of both the enhanced reduction of GO and increased microcracks to the excellent performance of the strain sensor. Recently, Hepp et al. laser-patterned PET to fabricate turbostratically graphitized carbon films as bending or mechanical pressure sensors.[183] The resultant sponge-like porous films showed a quantitative and reversible change in resistance upon bending or applying a pressure in normal loading direction. The compression or tension of the turbostratically graphitized domains led to reversible increase or decrease in resistance.

To simplify the fabrication process of high-sensitive and wide-linear-range pressure sensors, Du et al. introduced laser-scribed hierarchical microstructures into the as-fabricated flexible pressure sensor using a femtosecond laser.[184] These laser-texturing hierarchical microstructures composed of periodical pyramids with different sizes play important roles in improving sensor performance. The final pressure sensor exhibited a linear range from 27 to 65 kPa with a sensitivity of 0.86 kPa^{-1}, a rapid response to pressure changes within 7 ms, and excellent repeatability over 1000 cycles. These outstanding performances endowed the piezoresistive sensor with the detecting ability of human physiological signals such as wrist pulse, weak/deep breath, and imitated static tremors. As for the essential movement monitoring for training activities and human-machine interfaces, the nano/microcracks on the convex surface of joints for motion sensors require a facile and high-precise form for ultrawide detectable angle range and high angle sensitivity. Inspired by crack-shaped slit sensilla of scorpions with the capability of allowing the conversion of compression strain from external mechanical vibrations, Duan et al. engraved parallel periodic two-body tissue phases composed of MXene-coated PU hard blocks and soft air gaps using a laser to construct controlled slit structures.[185] Due to the presence of the biomimetic slit geometry and contexture resulting in ultrasensitivity, the obtained conformal motion sensors exhibited high sensitivity, ultralow angle detection threshold, fast response/relaxation times, wide range, and durability over 1000 cycles. The slit ratio controlled by laser-engraving parameters had a key effect on their performances such as sensitivity and minimum angle detection threshold. In short, a large number of as-reported studies reveal that laser-textured micro/nanostructures in the sensors could make them present broad pressure sensing range, high sensitivity, and rapid response speeds, thus improving their sensing performance for respective use.

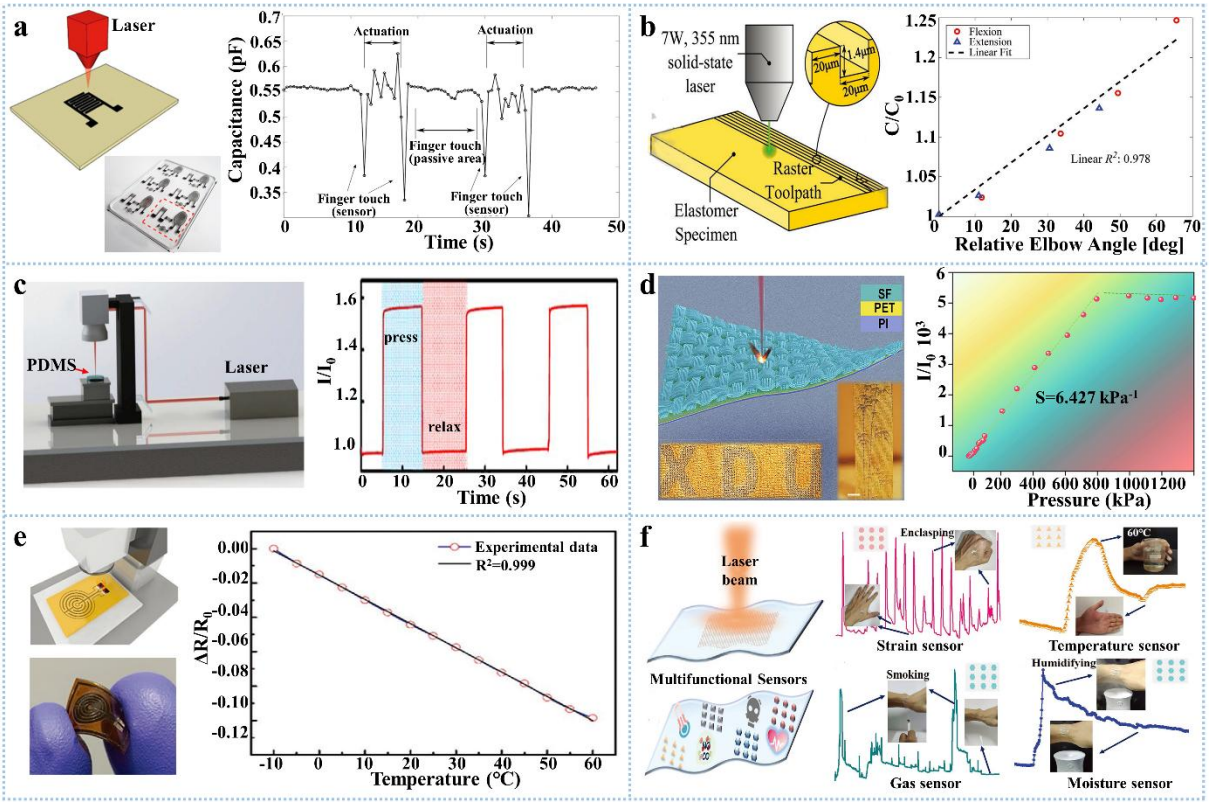

Figure 9. Physical sensing using laser micro/nanostructuring materials. a) The electrode patterned for interdigitated transducer geometries produced by using CO_2 laser ablation, which responds to finger touches directly on the sensor region. When the capacitance falls below 0.48 pF (corresponding to a valid touch input), a 2 kV periodic voltage input is applied to the actuator until a second touch input is detected. Reproduced with permission.[173] Copyright 2015, American Chemical Society. b) Schematic diagram of the laser raster process of the electrodes for highly stretchable and soft capacitance-based strain sensors, showing obvious capacitance change while bending the strain sensor at the elbow joint. Reproduced with permission.[174] Copyright 2017, Wiley-VCH. c) The fabrication schematic of micro-structured PDMS for wearable pressure sensors with a laser micro-engineering system. The micro-structuring sensor shows obvious sensing behavior under pressure. Reproduced with permission.[175] Copyright 2019, IOP Publishing. d) Schematic illustration of laser-engraved process of the silver-coated fabric as the integrated electrode of a sensor with various patterns. The obtained flexible sensor shows a relative current variation as a function of time for applied stress from 0 to 1400 kPa. Reproduced with permission.[177] Copyright 2020, the authors, published by Springer Nature. e) Laser-induced temperature sensor showing good resistance response under different temperature ranges from -10 to 60 °C. Reproduced with permission.[179] Copyright 2020, Wiley-VCH. f) Femtosecond laser direct writing of graphene patterns for multifunctional sensors, which show corresponding resistance change with time under the certain conditions of griping, holding a beaker with hot water (60 °C), smoking and humidifying. Reproduced with permission.[180] Copyright 2020, Wiley-VCH.

3.4 Biosensing

In terms of health monitoring, medical diagnosis, and disease treatment, sensitive and specific detection of expressing biomolecules is of paramount significance, which could obtain physiological information from living organisms and offer the state of life activities. As a result, the related device, termed as biosensors, has been extensively explored for various biological substances such as bacteria, pathogens, and virus microorganisms in the surroundings as well as the metabolites like glucose, lactic acid, and dopamine inside human body (Table 4). Recently, portable and rapid detection of cancer-associated biomarkers, such as proteins, antibodies, hormones, cytokines, prions, DNA or RNA in biofluids, poses an innovated need for smart biosensors. It is accepted that the performance of these biosensors is largely determined by the used sensing materials and their structures. To explore a new structuring strategy and novel materials is imperative. The emergence of the laser processing method offers a promising solution to the structure design of a biosensor for performance improvement.

Table 4. Performance, structure feature, and applications of biosensors obtained by various laser micro/nanostructuring strategies.

Materials	Mechanism	Laser parameters	Sensitivity and response	Micro/nanostructures	Targets	Applications	Ref
MIP, PI	ECR	CO_2 laser (1000 dpi/in, 5.5 W)	-13.32 μA/decade (0.05-100 μM AMOX) 1.356 μA/decade (1.5-4 mM AA)	Pattern with 3D porous structure	AMOX AA	Multi-detection systems	133
PET film	ECR	Pulsed laser	53.1 mV/dec (10-160 mM Cl^-) 33.1 mV/dec (0.25-2 mM Ca^{2+})	Patterned microfluidic structures (Spacing: 190 nm)	Cl^- Ca^{2+}	Point-of-care non-invasive lab-on-skin devices	155
Au/Ag-COC	SERE	Near IR CW laser (940 nm, 50 W)	300 pmol (0.001-10 mM) 10 s	Periodic nanopillar arrays	Adenosine	Miniaturized lab-on-a-chip devices	187
Ag NPs, GO	SERE	Near-IR laser (780 nm, 200 mW)	10^{-6} M 1 min	Highly porous structure	30-base ssDNA	SERS-active biochips	188
PEDOT: PSS, MIPs	ECR	fs laser (808 nm, 500 mW)	2.68 A/dec (0.01-10.0 M) LOD: 1 pg/ml	Patterned microcapillary channel arrays	Cortisol	Sweat-based sensor	189
PMMA	ECR	100 W laser	119 nA/(ng/ml) (100 pg/ml-100 ng/ml)	3D cuboidal pillars	Protein marker	On-chip Electrochemical biosensor	190
Cu nanocubes Kapton	ECR	ms UV laser (400-450 nm, 50 ms, 500 mW)	4532.2 μA/mM cm^2 LOD: 250 nM (0.025-4 mM)	Interconnected nano-sheet units (Length: 20 μm)	Glucose	Electrochemical biosensor	191

			< 3 s				
MXene/ PB, lignin	ECR	CO_2 laser (10.6 μm, 1000 dpi/in, 2.1-3.6 W)	49.2, 21.6, 5.78 μA/mM cm^2 LOD: 0.3 μM (0.01-5.3 mM Glu) 0.5 μM (0-20 mM Lac)	3D interconnected porous network	Glucose Lactate Alcohol	Disposable & portable biosensors	192
PI, PET	ECR	CO_2 laser (1000 dpi/in, 2.75-3.75 W)	3.50 μA/μM cm^2 (UA) 0.61 μA/μM cm^2 (Tyr) LOD: 0.74 μM, 3.6 μM	Periodic 3D porous structure and circular patterns of microfluidic channels	UA Tyrosine (Tyr)	Wearable sensor	193
Pyrrole, propionic acid, PI	ECR	CO_2 laser (1000 dpi/in, 2.5 W)	LOD: 0.08 ng/mL (0.43-50.2 ng/mL)	Porous structure	Cortisol	Wearable and portable sensing platforms	194
Pt NPs, G	ECR	CO_2 IR laser (10.6 μm, 9.6 W)	4.622 μA/mM LOD: 300 nM (<2.1 mM)	Hierarchical porous structures (BET SA: ~340 m^2/g Pore sizes: <9 nm)	Glucose	Sweat glucose biosensor	195
PI thin films	ECR	CO_2 laser (3 W)	13 ± 7 CFU/mL (25-10^5 CFU/mL)	Patterned macro/meso-porous structure	*S. enterica*	Electrochemical biosensors	196
PI thin films	ECR	CO_2 laser (1000 dpi/in, 4-25% maximum power)	1080 μA/mM cm^2 3500 μA/mM cm^2 0-30 mM	Porous graphene structures (pore size: 1-5 μm)	Glucose	Glucose sensors, wearable electronics	197
SilkNCT	ECR	N.A.	6.3 nA/μM (25-300 M) 174.0 nA/mM (5-35 mM) 22.7 nA/μM (20-300 μM) 196.6 nA/μM (2.5-115 μM) 51.8 mV/decade (1.25-40 μM) 31.8 mV/decade (2.5-115 μM) LOD: 5 μM, 0.5 mM, 1 μM, 1 μM, 1 mM, 0.5 mM	Hierarchical porous structure and graphitic nanocarbon structure	Glucose Lactate AA UA Na+ K+	Wearable sweat analysis sensor	198
BDD	ECR	ns laser (1064 nm, 12 W)	2119 μA/cm^2 mM^{-1} LOD: 0.2 × 10^{-6} M < 1 s	Arrayed pits with 20-30 μm diameters	Glucose	Nonenzymatic glucose sensors	199
PI	ECR	CO_2 laser (1000 dpi/in, 4 W)	16.28 nA mL/ng	Patterned porous graphene	CRP	Patient triage, telemedicine care, remote monitoring	200
2D MoS2	Resistance	CW Ar^+ laser (514 nm, 125-360 mW)	pg/mL level (2-2000 pg/mL) $\Delta R/R_a \approx 30\%$ <5 s	2H-MoS_2 array	SARS-CoV-2 protein	Point-of-use devices	201
PI film	ECR	CO_2 laser (6-15 W)	2.70 μM (10-200 μM) 1.29 μM (5-80 μM) 7.81 μM (25-250 μM)	Pattern of porous graphene structure	CAP Rac CLB	Portable analyzer, wearable sensors	202

Paper	Resistance	Nd:YAG CW laser (532 nm, 100 mW)	-0.15% ◦C^{-1} 0.0041% ppm^{-1} (TMA)	3D porous structure	Spoiled gas	Food spoilage monitoring	203

To solve expensive and time-consuming issue for fabricating miniaturized Raman-onchip biomolecular detection systems, Liu et al. used laser-assisted nano-replication to fabricate low-cost and large-area SERS substrates, thus significantly improving the sensitivity of on-chip Raman detection systems.[187] Such substrates consisting of gold-coated COC nanopillar arrays showed a SERS EF of up to ~10^7 because of the effect of the nanopillar diameter and interpillar spacing on the local electromagnetic field enhancement. When combining SERS technology with microfluidics, the label-free on-chip DNA detection can be achieved for further diagnosis of genetic disease. To better integrate SERS substrate with microfluidic devices and controllable contact with target molecules, Han et al. utilized a facile laser scribing method (780 nm, 200 mW) to fabricate Ag NPs@GO composite with hierarchical porous structures with the line width resolution of 20 μm as a reusable SERS sensor for DNA detection (Figure 10a).[188] Programmable laser scribing caused direct patterning of sensitive SERS channels. Together with the noncovalent interactions between DNA and graphene, it enabled efficient on-chip SERS detection and the regeneration of the biochip. In a similar way, Parlak et al. developed a laser-patterned microcapillary channel array and integrated it with the sensor together.[189] Laser-patterned microcapillary channels provided fast and precise delivery of sweat directly to the sensor interface. The resultant wearable sweat sensor could measure cortisol concentration in a real human sweat sample collected during exercise, showing noninvasiveness, ease-operation, and user-comfort features. These merits enabled the sensor to selectively detect various molecules, especially noncharged biomolecules and hormones. Consequently, laser-engraving microchannels could greatly improve the sensing performance of the sensor due to large surface area and capillary effect, which had been integrated into various devices. To improve the signal sensitivity with low background noise, off-surface matrix is employed for fabricating integrated sensor chip for biosensing. Arya et al. developed off-surface 3D matrix by a laser-engraving PMMA sheet, which was modified with antibodies in separate location for on-chip electrochemical biosensing protein marker in complex undiluted serum sample.[190] Such a biosensor platform has great potential to replace most commonly used optical ELISA-based detection platforms.

Considering the advantages of laser-engraving/scribing porous graphene for sensing electrodes, Tehrani et al. fabricated direct-laser-engraved units with a lateral length of roughly 20 μ m using a UV laser (400-450 nm, 50 ms, 500 mW).[191] Being decorated with pulse deposited copper nanocubes, they could act as a highly sensitive disposable glucose sensor strip. This fabrication not only resulted in high reproducibility (96.8%), stability (97.4%) and low cost, but also allowed for a high degree of flexibility and controllable electrode size. The resulting sensors showed excellent selectivity and sensitivity, low LOD, and suitable linear range for glucose detection in tear, saliva, and/or sweat. Lei et al. laser-scribed a lignin-based precursor to prepare highly conductive hierarchical nitrogen-doped graphene using a CO_2 laser (10.6 μm, 1000 dpi/in, 2.1-3.6 W) (Figure 10b).[192] Such a laser-scribed graphene with the interconnected carbon network displayed enhanced electrochemical activity with improved heterogeneous electron transfer rate due to its high conductivity and enriched active edge-plane sites. When modified with the $Ti_3C_2T_x$/PB, the resultant electrodes functionalized with catalytic enzymes could detect glucose, lactate, and alcohol, exhibiting remarkably enhanced electrochemical activity toward these biomarkers. Yang et al. utilized a CO_2 laser-cutting machine to fabricate entirely laser-engraving sensor, which could wirelessly and continuously monitor UA, tyrosine (Tyr), and vital signs.[193] The combination of LIG chemical sensor and laser-engraving microfluidic device facilitated continuous sweat sampling. The fast electron mobility, elevated current density and extended surface area enabled this graphene-based sensor to detect UA and Tyr in human sweat rapidly and accurately as well as monitor temperature and respiration rate (Figure 10c). Torrente-Rodríguez et al. exploited the exceptional performance of LIG for electrochemical sensing to achieve a flexible sensor array with a highly sensitive, selective, and efficient cortisol sensing ability (Figure 10d).[194] This LIG-based sensor electrode demonstrated a much higher sensitivity with 6- and nearly 2-fold reduction in current density of 0.0-1.0 ng/mL as compared with screen-printed carbon electrodes and glassy carbon electrodes, respectively. Due to the good immobilization ability of various proteins, such as enzymes, antibodies, and receptors, Yoon et al. modified porous LIG using acetic acid treatment via a dipping technique.[195] This simple modification treatment dramatically increased the ratio of carbon-carbon bonds to effectively enhance conductivity and decrease sheet resistance. After immobilizing chitosan-glucose oxidase composite, the LIG composite electrode exhibited a high sensitivity of 4.622 μA/mM as well as an ultra-low LOD. With a growing concern on food-

borne illnesses, a rapid, sensitive, and inexpensive techniques for pathogen detection is a critical need. To use low-cost nanomaterials to increase detection sensitivity of the electrodes in the biosensors, Soares et al. fabricated a highly sensitive and label-free LIG electrode by laser induction on the PI film in ambient conditions.[196] Followed by the functionalization of *Salmonella* antibodies, it could electrochemically quantify the food-borne pathogen *Salmonella enterica serovar Typhimurium* in chicken broth across a wide linear range of 25 to 10^5 CFU/mL, showing a low LOD of 13 ± 7 CFU/mL and an average response time of 22 min (Figure 10e). The resulting LIG sensors displayed high selectivity as demonstrated by an insignificant response to other bacteria strains. Given the significance of 3D porous structures in improving the sensitivity of the sensors for the detection of a trace amount of analyte in biofluids, Zhu et al. deposited the uniform nickel and gold layer on LIG electrodes, which demonstrated a significantly enhanced sensitivity and a large linear range for sensing glucose.[197] The porous LIG foam with a pore size of about 1-5 μm enabled the sensor to exhibit a high sensitivity. Utilizing the similar laser-engraving technique to treat other substrates, He et al. fabricated the electrochemical sensor array based on silk fabric-derived nitrogen-doped carbon textile.[198] After being integrated onto flexible patch, it could not only simultaneously detect six biomarkers including glucose, lactate, AA, UA, Na^+, and K^+, but also show high sensitivity, good selectivity, and long-term stability. To achieve robust and high-performance electrochemical sensing electrodes, Gao et al. combined high-speed laser-engraving and pulsed electrodeposition of Cu nanostructures to fabricate a hierarchical nonenzymatic glucose sensing electrode on BDD.[199] Owing to the d-band catalytic activity of the Cu nanoflake with the low capacitive background current of the engraved BDD substrate, the hierarchical nanostructured electrode enabled fast, precise, and high signal-to-noise ratio detection of trace glucose, showing a high sensitivity, ultrafast response time, and low DOL (Figure 10f). Besides, excellent cyclicality and anti-interference ability made the sensor to be great stability for practical usage.

In recent years, the COVID-19 pandemic has highlighted the importance and urgent need for rapid and accurate diagnostic tests. In view of outstanding improvement in the sensing performance of laser-textured micro/nanostructures, the sensors produced by this technology have been widely used for the determination of various biomarkers in a time-effective and cost-effective way. Torrente-Rodríguez et al. prepared laser-engraved graphene as four electrodes of

multiplexed electrochemical sensors after being functionalized with antibodies or coating proteins specific to each analyte.[200] The resultant sensor could measure the concentration of four analytes: SARS-CoV-2 nucleocapsid protein, C-reactive protein, and SARS-CoV-2 spike protein immunoglobulins S1-IgM and S1-IgG within minutes, finally diagnosing COVID-19 and determining which stage of infection the patient (Figure 10g). To meet the increasing requirement of COVID-19 pandemic, multiplex electronic antigen sensors for the detection of SARS-COV-2 spike glycoproteins are applied recently. Muratore et al. utilized CW Ar^+ laser to anneal amorphous MoS_2, finally creating an array of semiconducting 2H-MoS_2 transducer regions.[201] After this semiconducting crystalline region was functionalized with monoclonal antibody fragments, the obtained sensor array on a single chip could detect analyte concentrations across six orders of magnitude from pg/mL to μg/mL. Recently, Jung et al. used a 532 nm Nd:YAG CW laser to irradiate various papers to prepare LIG sensors with porous structures for wireless and real-time monitoring of the food status based on the chemical-/thermo-sensing capabilities of LIG. By optimizing laser irradiation conditions, the temperature and chemical gas coefficient of resistance change were improved to 0.15%$\cdot C^{-1}$ and 0.0041% ppm^{-1}, respectively.[203] To sum up, laser micro/nanostructuring technology has made great progress for biosensing applications. However, the gradual development of health concept and the evolved pathogens require the innovated sensing mechanism and novel micro/nanostructuring sensing materials.

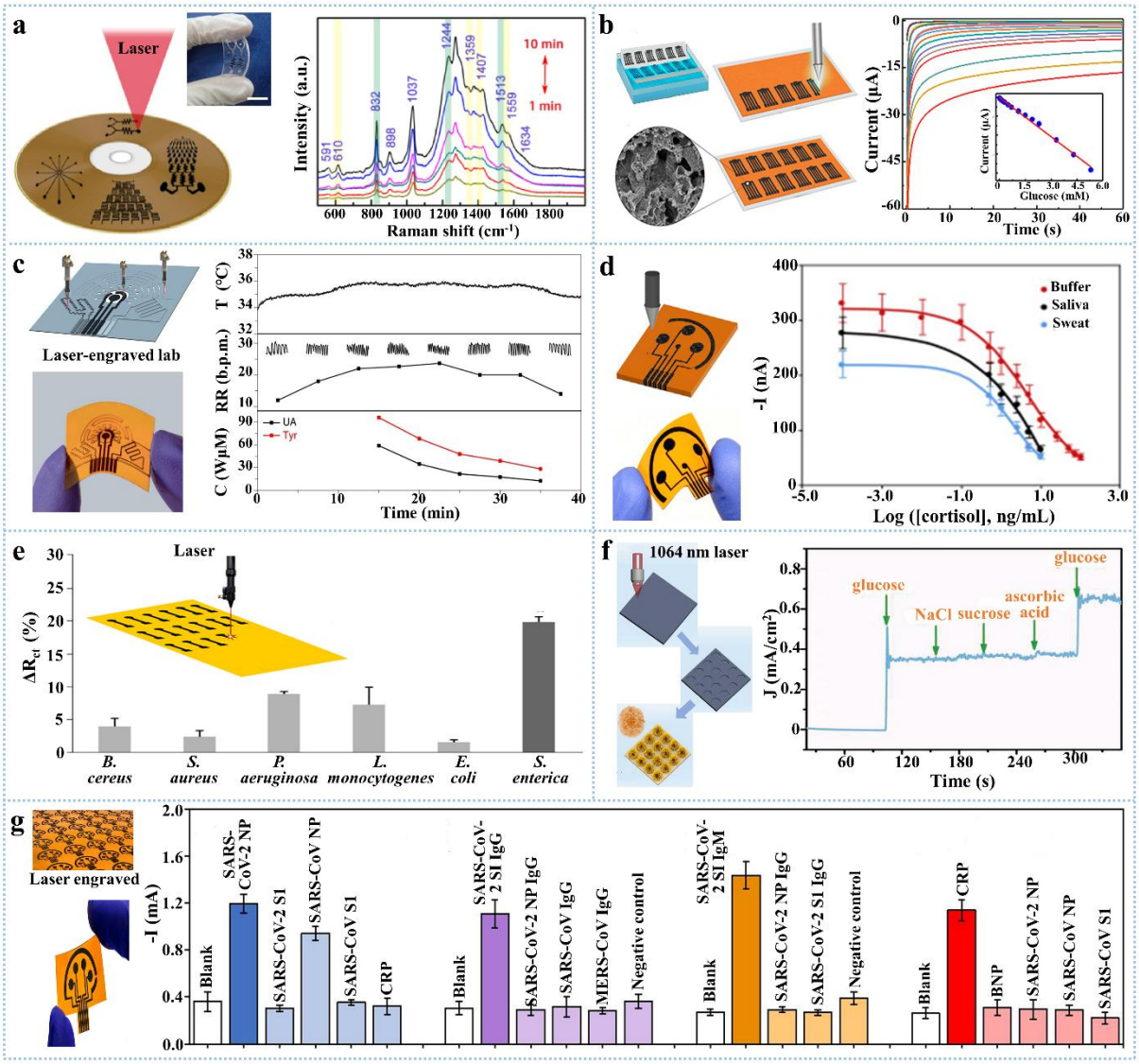

Figure 10. Biosensing performance of laser micro/nanostructuring materials. a) Direct laser scribing of Ag NPs@rGO biochip as a reusable SERS sensor for DNA detection, showing obvious SERS detection signals within 1 min with a concentration of 10^{-6} M unchanged. Reproduced with permission.[188] Copyright 2018, Elsevier. b) The direct-write-laser-scribing fabrication of nitrogen-doped laser-scribed graphene, showing a high electrochemical sensitivity to glucose. Reproduced with permission.[192] Copyright 2019, American Chemical Society. c) The entirely laser-engraved sensor composed of the laser-scribing microfluidic module and the laser-engraved graphene-based chemical and physical sensors, which could perform real-time, continuous *in situ* monitoring for respiration rate (RR), temperature and sweat UA and Tyr levels. Reproduced with permission.[193] Copyright 2019, Nature Publishing Group. d) Laser-engraving graphene platform for a disposable flexible graphene sensor array, presenting no significant slope variation between data obtained in human biospecimens or in buffered solutions as well as LOD of 0.08 ng/mL in sweat and saliva samples. Reproduced with permission.[194] Copyright 2020, Elsevier. e) LIG electrodes on the PI film as

electrochemical immunosensors, whose percentage charge transfer resistance shows obvious change at a constant concentration (10^4 CFU/mL) of different interferent bacteria and *S. enterica Typhimurium*. Reproduced with permission.[196] Copyright 2020, American Chemical Society. f) Schematic diagram of high-speed laser-engraved BDD and deposited Cu nanoflake as electrodes for copper catalyzed non-enzymatic glucose sensing, showing a good response to continuously dripping glucose and interfering substances. Reproduced with permission.[199] Copyright 2022, Wiley-VCH. g) Mass-producible laser-engraved graphene arrays for a disposable and flexible graphene sensor, presenting selective response to NP, S1-IgG and S1-IgM isotypes, and CRP sensors against different non-target circulating analytes.[200] Reproduced with permission.[200] Copyright 2020, Elsevier.

4. Outlook and Perspectives

As an ultrafast and ultraprecise technique, laser micro/nano-structuring fabrication has gradually become a versatile processing method for advanced smart electronic devices, owing to its high precision, controllability, quality, flexibility of structural design, and good compatibility with various materials. Past twenty years have witnessed its great evolution and wide interdisciplinary with sensors and sensing applications, also heralding a multidisciplinary trend, as illustrated in Figure 11. In this review, beginning with brief introduction to a series of pulsed-laser processing methods for micro/nanostructuring, sensing applications of laser-treated micro/nanostructures towards chemical analytes, physical stimuli, and biomarkers based on the discussion of common sensing mechanisms were comprehensively illustrated. These laser micro/nanostructuring materials or devices toward high-performance sensing applications, including high sensitivity, broad working range, and outstanding durability, are prominently stated. A detailed analysis of various laser-engineered micro/nanostructures with unique sensing performances is compared to demonstrate the advantages of laser-enabled fabrication over other fabrications and provide possible solutions to the size limitation problem of high-performance miniature sensors.

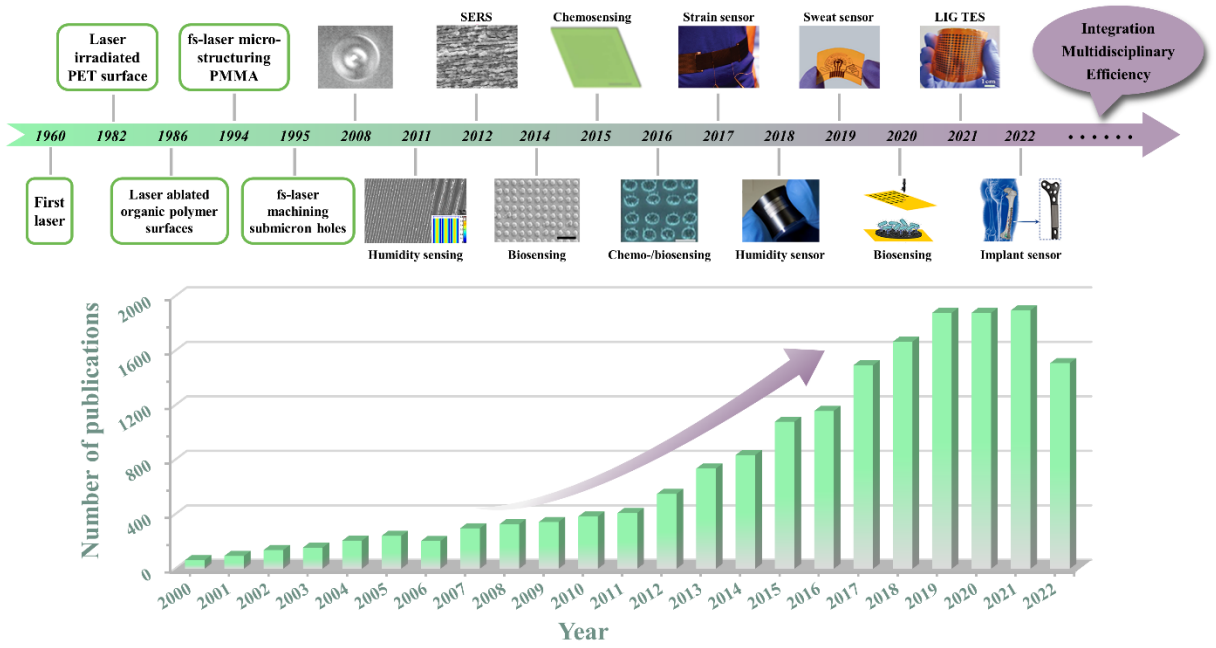

Figure 11. A brief timeline and representative designing of laser-processing micro/nanostructures for sensing applications, in combination with the number of publications regarding "laser structuring" and "sensor" and "sensing" during past about twenty years from Web of Science. The panels are reproduced with permission.[74,77,120,135,158,159,164,174,187,193,196,204] Copyright 2014, 2016, 2018, and 2020, American Chemical Society. Copyright 2011, Elsevier. Copyright 2012, 2015, 2017, 2021 and 2022, Wiley-VCH. Copyright 2008 and 2019, Nature Publishing Group.

Although the improved processing accuracy and processing quality considerably bring outstanding achievements in sensing applications of laser-texturing micro/nanostructures, the rapid developments in sensing industry have induced new challenges for laser micro/nanostructuring sensors with high performance for various analytical applications.

Firstly, it is demonstrated in above studies that the laser structuring sensors integrated with diverse morphologies and geometries are more sensitive to specific external stimuli because distinctive geometrical configurations exhibit different responding performances. However, the single-scale microstructures on the sensor often display good robustness but fail to meet the requirements of both broad sensing range and high sensitivity. Hierarchal structures with microscale, submicron scale, or nanoscale on the sensor provide enhanced sensing range and sensitivity simultaneously but have poor stability due to easily damaged submicron scale and nanoscale structures. Thus, the trade-offs between different features have hampered the development of efficient laser-micro/nanostructuring sensors with both multiscale and robustness as well as simultaneous and parallel properties. Additionally, the modulation of these

geometries of the hybrid structures with multiple dimensions is challenging via a single laser structuring for better tuning the linearity, sensitivity, and sensing range.

Secondly, despite the exceptional compatibility with soft and hard materials in various applications, the exploration of the interaction between laser and material is still very limited. In particular, the potential mechanism behind their interaction from a microscopic point of view is unclarified and controversial. These limitations bring a confusing understanding of the principle of laser micro/nanofabrication, finally resulting in the unsatisfactory resolution of the formed micro/nanostructures. As reported, the intrinsic optical diffraction limit restricts the further improvement of laser processing accuracy despite significant breakthroughs in manufacturing accuracy. Accordingly, the stagnation and hindrance in the study on the mechanisms affect the size of the sensor structure largely, thereby impairing the sensing performance.

Thirdly, as an ultrafast fabrication, the common laser processing, especially short-duration pulse laser processing, mainly exploits the point-by-point single-thread scanning method, thus leading to low processing efficiency. For example, several hours are required to construct submicron structures on the glass substrate with 1×1 cm^2 area using a femtosecond laser. Moreover, this laser-structuring showed low yield compared with chemical methods. Consequently, these drawbacks inhibit its mass production and industrial applications. How to overcome low efficiency and poor yield while ensuring the processing quality is challenging. With the development of laser high-resolution time-domain/space-domain/frequency-domain shaping technology, the processing efficiency is improved by optimizing the scanning mode and multi-focus parallel processing, thus vacillating the high efficiency, high precision, high quality, and high quality of the micro/nanostructures. The rise of large-area and high-consistency laser manufacturing is expected and explored to innovate the limitations of sensor performance.

Last but not least, harnessing the multimodal sensing strategy becomes a challenge in developing high-performance sensors with the rising demands of complex application scenarios. Although the utilization of laser processing has achieved multi-sensing functions and multi-sensor integration in a single device, the integrated sensor or device is still in its infancy and has unsatisfactory or limited sensing performance owing to the limitation of laser manufacturing. Moreover, complex scenarios require the sensors with additional functions like

self-cleaning, self-powering, and self-healing functions. In view of the outstanding contributions of laser micro/nanostructuring to extremely wetting surface engineering, the laser-treated micro/nanostructures enable the sensor to show high-performance sensing and be applied in a more complex and extreme environment. In short, the presence of these challenges only limited the development of laser micro/nanostructuring sensing temporarily. Continuous emphases on them will dramatically facilitate the development of the next generation of micro/nano sensors.

Nowadays, the whole world is facing a lasting and changeable COVID-19 pandemic, posing great demands on portable and high-efficient sensors. With the breakthrough of laser micro/nanostructuring fabrication in the sensing field, more problems are solved gradually. These progress in turn boost the multidisciplinary of laser processing with other disciplines and technologies, offering abundant solutions to circumvent challenges such as mechanism, efficiency, and integration. On the one hand, *in situ* self-powered sensors have become a new development direction. The use of laser processing enables the integration of other devices with sensors into one to realize multifunctional sensors through a well combination of additive and subtractive manufacturing using a high-precision laser instead of complex multistep chemical synthesis. Moreover, inspired by multifunctional integration existing inside natural organisms originated from unique diverse structures in hierarchical, porous, and periodic ways, the fusion of flexible laser micro/nanostructuring and bionics would enable the production of hierarchical micro/nanostructures with better robustness and even self-healing in a sensor. Such an intercrossing combination not only achieves the laser-processing structure requirement for good sensing performance, but also extends laser micro/nanostructuring to multimodal sensing applications. On the other hand, it is necessary to innovate laser technology to improve the fabrication precision of the micro/nanostructures for high integration while keeping the sensitivity. So, the innovation of lasers with different parameters will promote the emergence of new sensors, opening up a whole new set of intelligent products. Their fantastic sensing applications will bring humanity to move one step closer to a new era of intelligence.

Abbreviations

Acetylcholinesterase (AChE)

Ammonium nitrate (AN)

Amoxicillin (AMOX)

Argon-ion (Ar^+)

Ascorbic acid (AA)

Boron-doped diamond (BDD)

Black phosphorus (BP)

Carbon-fiber-reinforced poly-ether-ether-ketone (CFR-PEEK)

Carbon network-forming agent (CNFA)

Chloramphenicol (CAP)

Clenbuterol (CLB)

Continuous wave (CW)

C-reactive protein (CRP)

Cyclic olefin copolymer (COC)

Density per inch (DPI)

Dinitrotoluene (DNT)

Diode-pumped solid-state (DPSS)

Dopamine (DA)

Electrochemical reaction (ECR)

Enhancement factor (EF)

Enzyme linked immunosorbent assay (ELISA)

Extracellular vesicles (EVs)

Gauge factor (GF)

Graphene oxide (GO)

Heat-affected zone (HAZ)

High spatial frequency (HSFL)

Human-machine interactions (HMI)

Infrared (IR)

Internet of Things (IoT)

Laser-induced graphene (LIG)

Laser-induced nanostructuring of SERS-active thin films (LINST)

Limit of detection (LOD)

Liquid metal (LM)

Lead zirconate titanate (PZT)

Localized surface plasmon resonance (LSPR)

Low spatial frequency (LSFL)

Mercaptobenzoic acid (MBA)

Methylene blue (MB)

Molecularly imprinted polymer (MIP)

Nanoparticles (NPs)

Nucleocapsid protein (NP)

Nanostructures (NSs)

One-dimensional (1D)

Organophosphorus (OPs)

Picric acid (PA)

Picosecond direct laser interference patterning (ps-DLIP)

Picosecond direct laser writing (ps-DLW)

Polyaniline (PANI)

Polyethylene terephthalate (PET)

Poly-ether-ether-ketone (CFR-PEEK)

Polydimethylsiloxane (PDMS)

Polyimide (PI)

Polymethyl methacrylate (PMMA)

Poly(lactic-co-glycolic acid) (PLGA)

Polystyrene (PS)

Polyvinylidene fluoride (PVDF)

Polyvinylpyrrolidone(PVP)

point-of-care test (POCT)

Prussian blue (PB)

Ractopamine (Rac)

Rhodamine 6G (Rh6G)

Rhodamine 101 (R101)

Reduced graphene oxide (rGO)

Surface enhanced fluorescence effect (SEFE)

Surface enhanced photoluminescence (SEPL)

Surface enhanced Raman effect (SERE)

Surface enhanced Raman scattering (SERS)

Surface-enhanced photoluminescence (SEPL)

Surface-plasmon resonance (SPR)

Terahertz (THz)

Triboelectric sensor (TES)

Triboelectric sensing array (TSA)

Trinitrophenol (TNP)

Three-dimensional (3D)

Trimethylamine (TMA)

Two-beam-laser interference (TBLI)

Two-dimensional (2D)

Ultraviolet (UV)

Uric acid (UA)

Volatile organic compounds (VOC)

Acknowledgements

The authors thank Mr. Xiaohu Xia for the modification of Figure 11. This work was supported by National Natural Science Foundation of China (No. 52175550 and 22102104). Natural Science Foundation of Shenzhen University with grant No. 000002110712, Natural Science Foundation of Shenzhen Science and Technology Commission with grant No. RCBS20200714114920190, Guangdong Basic and Applied Basic Research Foundation (2021A1515010672) as well as the Bagui Scholarship project of Guangxi Zhuang Autonomous Region.

Conflict of Interest

The authors declare no conflict of interest.

References

[1] Z. Shi, L. Meng, X. Shi, H. Li, J. Zhang, Q. Sun, X. Liu, J. Chen, S. Liu, *Nano-Micro Lett.* **2022**, *14*, 141.

[2] R. X. Duan, X. D. Lou, F. Xia, *Chem. Soc. Rev.* **2016**, *45*, 1738.

[3] A. Tong, T. C. Sorrell, A. J. Black, C. Caillaud, W. Chrzanowski, E. Li, D. Martinez-Martin, A. McEwan, R. Wang, A. Motion, A. C. Bedoya, *Nat. Biotechnol.* **2021**, *39*, 144.

[4] D. J. Joe, S. Kim, J. H. Park, D. Y. Park, H. E. Lee, T. H. Im, I. Choi, R. S. Ruoff, K. J. Lee, *Adv. Mater.* **2017**, *29*, 1606586.

[5] Z. Lin, M. Hong, *Ultrafast Sci.* **2021**, 9783514.

[6] Y. Song, C. Qu, M. Ma, Q. Zheng, *Small* **2020**, *16*, 1903018.

[7] G. Lee, M. Zarei, Q. Wei, Y. Zhu, S. G. Lee, *Small* **2022**, *18*, 2203491.

[8] Y. Zhang, L. Zhang, L. Yang, C. I. Vong, K. F. Chan, W. K. Wu, T. N. Kwong, N. W. Lo, M. Ip, S. H. Wong, J. J. Sung, *Sci. Adv.* **2019**, *5*, eaau9650.

[9] J. Zhang, X. Liu, G. Neri, N. Pinna, *Adv. Mater.* **2016**, *28*, 795.

[10] S. Yang, C. Zhang, J. Ji, Y. Liu, J. Wang, Z. Shi, *Adv. Mater. Technol.* **2022**, 2200309.

[11] J. Park, Y. Lee, J. Hong, Y. Lee, M. Ha, Y. Jung, H. Lim, S. Y. Kim, H. Ko, *ACS Nano* **2014**, *8*, 12020.

[12] Y. Zhang, K. F. Chan, B. Wang, P. W. Y. Chiu, L. Zhang, *Sensor Actuat. B-Chem.* **2018**, *271*, 128.

[13] S. Song, C. Zhang, W. Li, J. Wang, P. Rao, J. Wang, T. Li, Y. Zhang, *Nano Energy* **2022**, *100*, 107513.

[14] N. Bai, L. Wang, Q. Wang, J. Deng, Y. Wang, P. Lu, J. Huang, G. Li, Y. Zhang, J. Yang, K. Xie, *Nat. Commun.* **2022**, *11*, 209.

[15] C. Zhang, M. Qu, X. Fu, J. Lin, *Small Methods* **2022**, *6*, 2101384.

[16] J. Zhang, Z. Qin, D. Zeng, C. Xie, *Phys. Chem. Chem. Phys.* **2017**, *19*, 6313.

[17] N. Wongkaew, M. Simsek, C. Griesche, A. J. Baeumner, *Chem. Rev.* **2018**, *119*, 120.

[18] R. X. Duan, X. L. Zuo, S. T. Wang, X. Y. Quan, D. L. Chen, Z. Chen, L. Jiang, C. Fan, F. Xia, *J. Am. Chem. Soc.* **2013**, **135**, 4604.

[19] T. Zhou, T. Zhang, *Small Methods* **2021**, *5*, 2100515.

[20] Y. M. Jia, X. L. Zuo, X. D. Lou, M. Miao, Y. Cheng, X. Min, X. Li, F. Xia, *Anal. Chem.* **2015**, *87*, 3890-3894.

[21] Y. Xu, X. Wu, X. Guo, B. Kong, M. Zhang, X. Qian, S. Mi, W. Sun, *Sensors* **2017**, *17*, 1166.

[22] A. A. Lahcen, S. Rauf, T. Beduk, C. Durmus, A. Aljedaibi, S. Timur, H. N. Alshareef, A. Amine, O. S. Wolfbeis, K. N. Salama, *Biosens. Bioelectron.* **2020**, *168*, 112565.

[23] J. Yang, F. Luo, T. S. Kao, X. Li, G. W. Ho, J. Teng, X. Luo, M. Hong, *Light Sci. Appl.* **2014**, *3*, e185.

[24] F. Sima, K. Sugioka, *Nanophotonics* **2021**, *10*, 2389.

[25] H. Wang, Y. L. Zhang, W. Wang, H. Ding, H. B. Sun, *Laser Photonics Rev.* **2017**, *11*, 1600116.

[26] J. H. Park, H. E. Lee, C. K. Jeong, S. K. Hong, K. I. Park, and K. J. Lee, *Nano Energy* **2019**, *56*, 531.

[27] B. Zheng, G. Zhao, Z. Yan, Y. Xie, J. Lin, *Adv. Funct. Mater.* **2022**, 2210084.

[28] X. Liu, C. Xing, F. Yang, Z. Liu, Y. Wang, T. Dong, L. Zhao, H. Liu, W. Zhou, *Adv. Energy Mater.* **2022**, *12*, 2201009.

[29] Y. Chen, Y. Wang, J. Yu, G. Xiong, H. Niu, Y. Li, D. Sun, X. Zhang, H. Liu, W. Zhou, *Adv. Sci.* **2022**, *9*, 2105869.

[30] H. Zeng, X. W. Du, S. C. Singh, S. A. Kulinich, S. Yang, J. He, W. Cai, *Adv. Funct. Mater.* **2012**, *22*, 1333.

[31] F. M. Vivaldi, A. Dallinger, A. Bonini, N. Poma, L. Sembranti, D. Biagini, P. Salvo, F. Greco, F. Di Francesco, *ACS Appl. Mater. Interfaces* **2021**, *13*, 30245.

[32] H. Palneedi, J. H. Park, D. Maurya, M. Peddigari, G. T. Hwang, V. Annapureddy, J. W. Kim, J. J. Choi, B. D. Hahn, S. Priya, K. J. Lee, *Adv. Mater.* **2018**, *30*, 1705148.

[33] W. Zhou, D. Bridges, R. Li, S. Bai, Y. Ma, T. Hou, A. Hu, *Sci. Lett. J.* **2016**, *5*, 228.

[34] A. Piqué, R. C. Auyeung, H. Kim, N. A. Charipar, S. A. Mathews, *J. Phys. D: Appl. Phys.* **2016**, *49*, 223001.

[35] T. H. Maiman, *Nature* **1960**, *187*, 493.

[36] M. J. Jackson. Microfabrication and Nanomanufacturing, CRC Press, New York 2005.

[37] R. Srinivasan and W. J. Leigh, *J. Am. Chern. Soc.* **1982**, *104*, 6784.

[38] E. Sutcliffe, R. Srinivasan, *J. Appl. Phys.* **1986**, *60*, 3315.

[39] W. Xiong, Y. Zhou, W. Hou, L. Jiang, M. Mahjouri-Samani, J. Park, X. He, Y. Gao, L. Fan, T. Baldacchini, J. F. Silvain, *Front. Optoelectron.* **2015**, *8*, 351.

[40] G. González-Rubio, A. Guerrero-Martínez, L. M. Liz-Marzán, *Acc. Chem. Res.* **2016**, *49*, 678.

[41] L. Yang, J. Wei, Z. Ma, P. Song, J. Ma, Y. Zhao, Z. Huang, M. Zhang, F. Yang, X. Wang, *Nanomaterials* **2019**, *9*, 1789.

[42] B. N. Chichkov, C. Momma, S. Nolte, F. Von Alvensleben, A. Tünnermann, *Appl. Phys. A* **1996**, *63*, 109.

[43] C. Momma, B. N. Chichkov, S. Nolte, F. von Alvensleben, A. Tünnermann, H. Welling, B. Wellegehausen, *Opt. Commun.* **1996**, *129*, 134.

[44] B. Jaeggi, B. Neuenschwander, M. Schmid, M. Muralt, J. Zuercher, U. Hunziker, *Phys. Procedia* **2011**, *12*, 164.

[45] V. Kumar, R. Verma, S. Kango, V. S. Sharma, *Materials Today Commun.* **2021**, *26*, 101736.

[46] B. Mao, A. Siddaiah, Y. Liao, P. L. Menezes, *J. Manuf. Process.* **2020**, *53*, 153.

[47] A. Ostendorf, G. Kamlage, U. Klug, F. Korte, B. N. Chichkov, Femtosecond versus picosecond laser ablation. In Photon Processing in Microelectronics and Photonics IV (Vol. 5713, pp. 1-8). SPIE, **2005**.

[48] S. Marimuthu, B. Smith, A. Kiely, Y. Liu, *CIRP J. Manuf. Sci. Technol.* **2020**, *28*, 107.

[49] R. Bathe, V. Sai Krishna, S. K. Nikumb, G. Padmanabham, *Appl. Phys. A* **2014**, *117*, 117.

[50] J. Zhou, H. Shen, Y. Pan, X. Ding, *Opt. Lasers Eng.* **2016**, *78*, 113.

[51] B. Bhattacharyya, B. Doloi, Modern Machining Technology **2020**, pp. 161-363.

[52] D. Zhu, P. Zhang, Z. Tian, C. Chen, X. Hua, S. Xu, X. Xie, *Appl. Sci.* **2020**, *10*, 9054.

[53] X. Jia, Y. Chen, H. Wang, G. Zhu, X. Zhu, *Opt. Laser Technol.* **2020**, *130*, 106351.

[54] T. Zhang, C. Zhang, L. Zhang, J. Li, *Opt. Commun.* **2021**, *482*, 126592.

[55] P. Pou, A. Riveiro, J. Del Val, R. Comesaña, J. Penide, F. Arias-González, R. Soto, F. Lusquiños, J. Pou. *Procedia Manuf.* **2017**, *13*, 694.

[56] P. Fan, M. Zhong, Handbook of Laser Micro-and Nano-Engineering, **2020**, pp.1-42.

[57] J. Xiao, P. Liu, C. X. Wang, G. W. Yang, *Prog. Mater. Sci.* **2017**, *87*, 140.

[58] E. Fazio, B. Gökce, A. De Giacomo, M. Meneghetti, G. Compagnini, M. Tommasini, F. Waag, A. Lucotti, C. G. Zanchi, P. M. Ossi, M. Dell'Aglio, *Nanomaterials* **2020**, *10*, 2317.

[59] S. X. Liang, L. C. Zhang, S. Reichenberger, S. Barcikowski, *Phy. Chem. Chem. Phy.* **2021**, *23*, 11121.

[60] N. Mintcheva, P. Srinivasan, J. B. B. Rayappan, A. A. Kuchmizhak, S. Gurbatov, S. A. Kulinich, *Appl. Surf. Sci.* **2020**, *507*, 145169.

[61] K. H. Leitz, B. Redlingshöfer, Y. Reg, A. Otto, M. Schmidt, *Phys. Procedia* **2011**, *12*, 230.

[62] S. Marimuthu, M. Antar, J. Dunleavey, *Int. J. Adv. Manuf. Technol.* **2019**, *102*, 2833.

[63] S. Marimuthu, J. Dunleavey, Y. Liu, M. Antar, B. Smith, *Opt. Laser Technol.* **2019**, *117*, 251.

[64] Y. Wang, X. Zhao, C. Ke, J. Yu, R. Wang, *Colloid Interface Sci. Commun.* **2020**, *35*, 100256.

[65] B. F. Mohazzab, B. Jaleh, A. Fattah-alhosseini, F. Mahmoudi, A. Momeni, *Surf. Interfaces* **2020**, *20*, 100597.

[66] L. B. Boinovich, E. B. Modin, A. R. Sayfutdinova, K. A. Emelyanenko, A. L. Vasiliev, A. M. Emelyanenko, *ACS Nano* **2017**, *11*, 10113.

[67] A. Samanta, W. Huang, H. Chaudhry, Q. Wang, S. K. Shaw, H. Ding, *ACS Appl. Mater. Interfaces* **2020**, *12*, 18032.

[68] L. Chen, H. Ping, T. Yang, T. Hu, P. Bennett, Z. Zheng, Q. Yang, W. Perrie, S. P. Edwardson, G. Dearden, D. Liu, *Mater. Res. Exp.* **2020**, *6*, 1250e2.

[69] L. B. Boinovich, M. E. Alexandre, D. M. Alexander, G. D. Alexandr, A. E. Kirill, *ACS Appl. Mater.*

Interfaces **2015**, *7*, 19500.

[70] J. Li, T. F. Chung, Y. P. Chen, G. J. Cheng, *Nano Lett.* **2012**, *12*, 4577.

[71] M. Zupančič, M. Može, P. Gregorčič, I. Golobič, *Appl. Surf. Sci.* **2017**, *399*, 480.

[72] J. Bonse, *Nanomaterials* **2020**, *10*, 1950.

[73] C. Paladiya, A. Kiani, *Sensor Actuat. B-Chem.* **2018**, *268*, 494.

[74] L. Guo, H. B. Jiang, R. Q. Shao, Y. L. Zhang, S. Y. Xie, J. N. Wang, X. B. Li, F. Jiang, Q. D. Chen, T. Zhang, H. B. Sun, *Carbon* **2012**, *50*, 1667.

[75] D. V. Ta, A. Dunn, T. J. Wasley, R. W. Kay, J. Stringer, P. J. Smith, C. Connaughton, J. D. Shephard, *Appl. Surf. Sci.* **2015**, *357*, 248.

[76] A. Kuchmizhak, S. Gurbatov, O. Vitrik, Y. Kulchin, V. Milichko, S. Makarov, S. Kudryashov, *Sci. Rep.* **2016**, *6*, 1.

[77] X. Hu, J. Huang, Y. Wei, H. Zhao, S. Lin, C. Hu, Z. Wang, Z. Zhao, X. Zang, *Adv. Sci.* **2022**, *9*, 2105499.

[78] Y. Li, M. Hong, *Laser Photon. Rev.* **2020**, ***14***, 1900062.

[79] Z. Chen, Y. Lin, Q. Qian, P. Su, Y. Ding, P. D. Tuan, L. Chen, D. Feng, *Desalination* **2022**, *528*, 115561.

[80] Y. Huang, L. Zeng, C. Liu, D. Zeng, Z. Liu, X. Liu, X. Zhong, W. Guo, L. Li, *Small* **2018**, *14*, 1803143.

[81] A. De Zanet, V. Casalegno, M. Salvo, *Ceram. Int.* **2021**, *47*, 7307.

[82] M. Wu, Y. Li, B. Yao, J. Chen, C. Li, G. Shi, *J. Mater. Chem. A* **2016**, *4*, 16213.

[83] K. Sun, H. Yang, W. Xue, A. He, D. Zhu, W. Liu, K. Adeyemi, Y. Cao, *Appl. Surf. Sci.* **2018**, *436*, 263.

[84] . Xing, Z. Li, H. Yang, X. Li, X. Wang, N. Li, *Mater. Design* **2019**, *183*, 108156.

[85] X. Wang, H. Zheng, Y. Wan, W. Feng, Y. C. Lam, *Engineering* **2018**, *4*, 816.

[86] Q. Pan, Y. Cao, W. Xue, D. Zhu, W. Liu, *Langmuir* **2019**, *35*, 11414.

[87] S. C. Vlădescu, C. Tadokoro, M. Miyazaki, T. Reddyhoff, T. Nagamine, K. Nakano, S. Sasaki, Y. Tsujii, *ACS Appl. Mater. Interfaces* **2022**, *14*, 15818.

[88] J. I. Ahuir-Torres, M. A. Arenas, W. Perrie, G. Dearden, J. De Damborenea, *Surf. Coat. Technol.* **2017**, *321*, 279.

[89] Z. Yu, G. Yang, W. Zhang, J. Hu, *J. Mater. Process. Technol.* **2018**, *255*, 129.

[90] Y. D. Chen, W. J. Tsai, S. H. Liu, J. B. Horng, *Opt. Laser Technol.* **2018**, *107*, 180.

[91] A. H. Hamad, High Energy and Short Pulse Lasers, **2016**, pp.21.

[92] C. Byram, S. S. B. Moram, V. R. Soma, *Analyst* **2019**, *144*, 2327.

[93] Z. Yan, D. B. Chrisey, *J. Photochem. Photobiol. C* **2012**, *13*, 204.

[94] C. Byram, S. S. B. Moram, A. K. Shaik, V. R. Soma, *Chem. Phys. Lett.* **2017**, *685*, 103.

[95] H. He, W. Cai, Y. Lin, B. Chen, *Chem. Commun.* **2010**, *46*, 7223.

[96] O. Olea-Mejía, M. Fernández-Mondragón, G. Rodríguez-de la Concha, M. Camacho-López, *Appl. Surf. Sci.* **2015**, *348*, 66.

[97] S. Park, J. Park, Y. G. Kim, S. Bae, T. W. Kim, K. I. Park, B. H. Hong, C. K. Jeong, S. K. Lee, *Nano Energy* **2020**, *78*, 105266.

[98] Y. Li, J. Long, Y. Chen, Y. Huang, N. Zhao, *Adv. Mater.* **2022**, *34*, 2200517.

[99] F. Kuisat, F. Ränke, R. Baumann, F. Lasagni, A. F. Lasagni, *Adv. Eng. Mater.* **2022**, *24*, 2101624.

[100] R. Srinivasan, E. Sutcliffe, B. Braren, *Appl. Phys. Lett.* **1987**, *51*, 1285.

[101] P. P. Pronko, S. K. Dutta, Squier, J., Rudd, J.V., Du, D. and Mourou, G., *Opt. Commun.* **1995**, *114*, 106.

[102] K. M. Davis, K. Miura, N. Sugimoto, K. Hirao, *Opt. Lett.* **1996**, *21*, *1729*.

[103] X. Tang, H. Liu, L. Xiao, M. Zhou, J. Fang, Z. Cui, H. Cheng, G. Li, Y. Zhang, M. Cao, *J. Mater. Chem. A* **2021**, *9*, 5630.

[104] Z. Cui, L. Xiao, Y. Li, Y. Zhang, G. Li, X. Tang, M. Zhou, J. Fang, L. Guo, S. Liu, M. Cao, *J. Mater. Chem. A* **2021**, *9*, 9719.

[105] X. He, G. Li, Y. Zhang, X. Lai, M. Zhou, L. Xiao, X. Tang, Y. Hu, H. Liu, Y. Yang, Y. Cai, L. Guo, S. Liu, and W. Zhao, *Chem. Eng. J.* **2021**, *416*, 129113.

[106] J. Zhang, S. Wang, L. Jiang, M. Wang, Z. Chu, W. Zhu, X. Li. *Appl. Sur. Sci.* **2020**, *502*, 144272.

[107] M. Zhou, X. He, X. Wu, L. Xiao, Z. Cui, X. Tang, L. Guo, S. Liu, H. Liu, Y. Zhang, G. Li, J. Zhu, *Appl. Mater. Today* **2020**, *21*, 100851

[108] S. Y. Liang, Y. F. Liu, S. Y. Wang, Z. K. Ji, H. Xia, B. F. Bai, H. B. Sun, *Adv. Funct. Mater.* **2022**, *32*, 0224957.

[109] W. Zhao, L. Xiao, X. He, Z. Cui, J. Fang, L. Xiao, C. Zhang, X. Li, G. Li, L. Zhong, Y. Zhang, *Opt. Laser Technol.* **2021**, *141*, 107115.

[110] S. Bai, D. Serien, A. Hu, K. Sugioka, *Adv. Funct. Mater.* **2018**, *28*, 1706262.

[111] J. Fang, Y. Zhang, L. Xiao, Y. Jiao, X. Tang, L. Xiao, Z. Cui, L. Luo, Y. Song, Y. Yang, T. Duan, *ACS Appl. Mater. Interfaces* **2021**, *13*, 14741.

[112] V. Vercillo, S. Tonnicchia, J. M. Romano, A. García-Girón, A. I. Aguilar-Morales, S. Alamri, S. S. Dimov, T. Kunze, A. F. Lasagni, E. Bonaccurso, *Adv. Funct. Mater.* **2020**, *30*, 1910268.

[113] M. Muthu, R. Pandey, X. Wang, A. Chandrasekhar, I. A. Palani, V. Singh, *Nano Energy*, **2020**, *78*, 105205.

[114] D. Tan, S. Zhou, J. Qiu, N. Khusro, *J. Photochem. Photobiol. C* **2013**, ***17***, 50.

[115] A. Y. Vorobyev, C. Guo, *Laser Photon. Rev.* **2013**, *7*, 385.

[116] Y. L. Zhang, Q. D. Chen, H. Xia, H. B. Sun, *Nano Today* **2010**, ***5***, 435.

[117] Y. Yu, S. Bai, S. Wang, A. Hu, *Engineering* **2018**, *4*, 779.

[118] K. Sugioka, *Inter. J. Extreme Manuf.* **2019**, *1*, 012003.

[119] A. I. Kuznetsov, A. B. Evlyukhin, M. R. Gonçalves, C. Reinhardt, A. Koroleva, M. L. Arnedillo, R. Kiyan, O. Marti, B. N. Chichkov, *ACS Nano* **2011**, *5*, 4843.

[120] R. Buividas, P. R. Stoddart, S. Juodkazis, *Ann. Phys. (Berlin)* **2012**, *524*, L5.

[121] H. Cheng, Y. Zhang, G. Li, X. Li, J. Fang, L. Xiao, X. Tang, Z. Cui, Y. Yang, Y. Cai, J. Zhu, *Opt. Laser Technol.* **2020**, *135*, 106719.

[122] L. Li, J. Zhang, Y. Wang, F. U. Zaman, Y. Zhang, L. Hou, C. Yuan, *InfoMat* **2012**, *3*, 1393.

[123] K. H. Ibrahim, M. Irannejad, B. Wales, J. Sanderson, M. Yavuz, K. P. Musselman, *Adv. Opt. Mater.* **2018**, *6*, 1701365.

[124] K. Ibrahim, I. Novodchuk, K. Mistry, M. Singh, C. Ling, J. Sanderson, M. Bajcsy, M. Yavuz, K. P. Musselman, *Small* **2019**, *15*, 1904415.

[125] S. Link, C. Burda, B. Nikoobakht, M. A. El-Sayed, *J. Phys. Chem. C* **2000**, *104*, 6152.

[126] F. Ye, D. Chang, A. Ayub, K. Ibrahim, A. Shahin, R. Karimi, S. Wettig, J. Sanderson, K. P. Musselman, *Chem. Mater.* **2021**, *33*, 4510.

[127] J. Zhang, M. Ren, Y. Li, J. M. Tour. *ACS Energy Lett.* **2018**, *3*, 677.

[128] W. Zhang, R. Li, H. Zheng, J. Bao, Y. Tang, K. Zhou, *Adv. Funct. Mater.* **2021**, *31*, 2009057.

[129] R. You, Y. Q. Liu, Y. L. Hao, D. D. Han, Y. L. Zhang, Z. You, *Adv. Mater.* **2020**, *32*, 1901981.

[130] L. R. Mingabudinova, A. S. Zalogina, A. A. Krasilin, M. I. Petrova, P. Trofimov, Y. A. Mezenov, E. V. Ubyivovk, P. Lönnecke, A. Nominé, J. Ghanbaja, T. Belmonte, *Nanoscale* **2019**, *11*, 10155.

[131] S. Song, S. H. Um, J. Park, I. Ha, J. Lee, S. Kim, H. Lee, C. H. Cheon, S. H. Ko, Y. C. Kim, H. Jeon, *ACS Nano* **2022**, *16*, 12840.

[132] R. Ye, D. K. James, J. M. Tour, Laser-induced graphene: from discovery to translation. Adv. Mater. 2019, **31**(1), 1803621.

[133] A. C. Marques, A. R. Cardoso, R. Martins, M. G. F. Sales, E. Fortunato, Laser-induced graphene-based platforms for dual biorecognition of molecules. *ACS Appl. Energy Mater.* **2020**, *3*, 2795.

[134] J. Lin, Z. Peng, Y. Liu, F. Ruiz-Zepeda, R. Ye, E. L. Samuel, M. J. Yacaman, B. I. Yakobson, J. M. Tour, *Nat. Commun.* **2014**, *5*, 1.

[135] Z. Yan, L. Wang, Y. Xia, R. Qiu, W. Liu, M. Wu, Y. Zhu, S. Zhu, C. Jia, M. Zhu, R. Cao, *Adv. Funct.*

Mater. **2021**, *31*, 2100709.

[136] B. Kulyk, B. F. Silva, A. F. Carvalho, P. Barbosa, A. V. Girão, J. Deuermeier, A. J. Fernandes, F. M. Figueiredo, E. Fortunato, F. M. Costa, *Adv. Mater. Technol.* **2022**, *7*, 2101311.

[137] L. Huang, J. Su, Y. Song, R. Ye, *Nano-Micro Lett.* **2020**, *12*, 1.

[138] S. A. Shafiee, S. C. Perry, H. H. Hamzah, M. M. Mahat, F. A. Al-lolage, M. Z. Ramli, *Electrochem. Commun.* **2020**, *120*, 106828.

[139] H. Wang, S. Delacroix, A. Zieleniewska, J. Hou, N. V. Tarakina, D. Cruz, I. Lauermann, A. J. Ferguson, J. L. Blackburn, V. Strauss, *Adv. Funct. Mater.* **2021**, *31*, 2104061.

[140] Z. T. Johnson, K. Williams, B. Chen, R. Sheets, N. Jared, J. Li, E. A. Smith, J. C. Claussen, *ACS Sens.* **2021**, *6*, 3063.

[141] S. Mishra, S. Mohanty, A. Ramadoss, *ACS Sens.* **2022**, *7*, 2495.

[142] J. Zhu, X. Huang, W. Song, *ACS Nano* **2021**, *15*, 18708.

[143] M. Wang, Y. Yang, W. Gao, *Trends Chem.* **2021**, *3*, 969.

[144] K. Xu, R. Zhou, K. Takei, M. Hong, *Adv. Sci.* **2019**, *6*, 1900925.

[145] S. D. Mahapatra, P. C. Mohapatra, A. I. Aria, G. Christie, Y. K. Mishra, S. Hofmann, V. K. Thakur, *Adv. Sci.* **2021**, *8*, 2100864.

[146] C. Chen, X. Wang, Y. Wang, D. Yang, F. Yao, W. Zhang, B. Wang, G. A. Sewvandi, D. Yang, D. Hu, *Adv. Funct. Mater.* **2020**, *30*, 2005141.

[147] T. Nguyen, T. Dinh, H. P. Phan, T. A. Pham, N. T. Nguyen, D. V. Dao, *Mater. Horiz.* **2021**, *8*, 2123.

[148] L. Duan, D. R. D'hooge, L. Cardon, *Prog. Mater. Sci.* **2020**, *114*, 100617.

[149] Y. Jian, W. Hu, Z. Zhao, P. Cheng, H. Haick, M. Yao, W. Wu, *Nano-Micro Lett.* **2020**, *12*, 1.

[150] A. Samanta, Q. Wang, S. K. Shaw, H. Ding, *Mater. Des.* **2020**, *192*, 108744.

[151] E. Bakker, M. Telting-Diaz, *Anal. Chem.* **2002**, *74*, 2781.

[152] P. L. Stiles, J. A. Dieringer, N. C. Shah, R. P. Van Duyne, *Annu. Rev. Anal. Chem.* **2008**, *1*, 601.

[153] J. D. Caldwell, O. Glembocki, F. J. Bezares, N. D. Bassim, R. W. Rendell, M. Feygelson, M. Ukaegbu, R. Kasica, L. Shirey, C. Hosten, *ACS Nano* **2011**, *5*, 4046.

[154] J. Wang, K. M. Koo, Y. Wang, M. Trau, *Adv. Sci.* **2019**, *6*, 1900730.

[155] B. P. Kunnel, S. Demuru, *Lab Chip* **2020**, *22*, 1793.

[156] B. Rai, R. Malmberg, V. Srinivasan, K. M. Ganesh, N. S. V. Kambhampati, A. Andar, G. Rao, C. B. Sanjeevi, K. Venkatesan, S. S. Ramamurthy, *ACS Sens.* **2021**, *6*, 4360.

[157] J. Plou, M. Charconnet, I. García, J. Calvo, L. M. Liz-Marzán, *ACS Nano* **2021**, *15*, 8984.

[158] J. Lu, J. H. Lu, H. Liu, B. Liu, L. Gong, E. S. Tok, K. P. Loh, C. H. Sow, *Small* **2015**, *11*, 1792.

[159] A. Kuchmizhak, E. Pustovalov, S. Syubaev, O. Vitrik, Y. Kulchin, A. Porfirev, S. Khonina, S. Kudryashov, P. Danilov, A. Ionin, *ACS Appl. Mater. Interfaces* **2016**, *8*, 24946.

[160] S. N. Erkızan, F. İdikut, Ö. Demirtaş, A. Goodarzi, A. K. Demir, M. Borra, I. Pavlov, A. Bek, *Adv. Optical Mater.* **2022**, 2200233, DOI: 10.1002/adom.202200233.

[161] H. Zhang, S. Wu, J. Liu, Y. Cai, C. Liang, *Phys. Chem. Chem. Phys.* **2016**, *18*, 22503.

[162] M. Sree Satya Bharati, C. Byram, V. R. Soma, *Front. Phys.* **2018**, *6*, 28.

[163] X. Lin, Z. Lu, W. Dai, B. Liu, Y. Zhang, J. Li, J. Ye, Laser engraved nitrogen-doped graphene sensor for the simultaneous determination of Cd (II) and Pb (II). *J. Electroanal. Chem.* **2018**, *828*, 41.

[164] J. Cai, C. Lv, E. Aoyagi, S. Ogawa, A. Watanabe, *ACS Appl. Mater. Interfaces* **2018**, *10*, 23987.

[165] M. Reynolds, L. M. Duarte, W. K. Coltro, M. F. Silva, F. J. Gomez, C. D. Garcia, *Microchem. J.* **2020**, *157*, 105067.

[166] B. Chen, Z. T. Johnson, D. Sanborn, R. G. Hjort, N. T. Garland, R. R. Soares, B. Van Belle, N. Jared, J. Li, D. Jing, E. A. Smith, *ACS Nano* **2021**, *16*, 15.

[167] N. F. Santos, S. O. Pereira, A. Moreira, A. V. Girão, A. F. Carvalho, A. J. Fernandes, F. M. Costa, *Adv. Mater. Technol.* **2021**, *6*, 2100007.

[168] R. Zhou, C. Wang, Q. Wang, L. Xie, Y. Ying, *Food. Anal. Methods* **2022**, *15*, 961.

[169] X. Liu, H. Cheng, Y. Zhao, Y. Wang, F. Li, *Biosens. Bioelectron.* **2022**, *199*, 113906.

[170] Y. Borodaenko, S. Syubaev, E. Khairullina, I. Tumkin, S. Gurbatov, A. Mironenko, E. Mitsai, E. Modin, E. L. Gurevich, A. A. Kuchmizhak, *Adv. Opt. Mater.* **2022**, *10*, 2201094.

[171] H. Nesser, G. Lubineau, *ACS Appl. Mater. Interfaces* **2021**, *13*, 36062.

[172] H. P. Phan, K. M. Dowling, T. K. Nguyen, T. Dinh, D. G. Senesky, T. Namazu, D. V. Dao, N. T. Nguyen, *Mater. Des.* **2018**, *156*, 16.

[173] O. A. Araromi, S. Rosset, H. R. Shea, *ACS Appl. Mater. Interfaces* **2015**, *7*, 18046.

[174] O. Atalay, A. Atalay, J. Gafford, H. Wang, R. Wood, C. Walsh, *Adv. Mater. Technol.* **2017**, *2*, 1700081.

[175] Y. Gao, C. Lu, Y. Guohui, J. Sha, J. Tan, F. Xuan, *Nanotechnology* **2019**, *30*, 325502.

[176] V. Palaniappan, S. Masihi, M. Panahi, D. Maddipatla, A. K. Bose, X. Zhang, B. B. Narakathu, B. J. Bazuin, M. Z. Atashbar, *IEEE Sens. J.* **2020**, *20*, 7605.

[177] H. Xu, L. Gao, Y. Wang, K. Cao, X. Hu, L. Wang, M. Mu, M. Liu, H. Zhang, W. Wang, Y. Lu, *Nano-Micro Lett.* **2020**, *12*, 159.

[178] Y. Gao, C. Yan, H. Huang, T. Yang, G. Tian, D. Xiong, N. Chen, X. Chu, S. Zhong, W. Deng, Y. Fang,

Adv. Funct. Mater. **2020**, *30*, 1909603.

[179] S. Gandla, M. Naqi, M. Lee, J. J. Lee, Y. Won, P. Pujar, J. Kim, S. Lee, S. Kim, *Adv. Mater. Technol.* **2020**, *5*, 2000014.

[180] X. Ye, M. Qi, Y. Yang, M. Yu, T. Huang, J. Zhang, X. Yuan, G. Suo, X. Hou, L. Feng, L. Zhang, *Adv. Mater. Technol.* **2020**, *5*, 2000446.

[181] A. Chhetry, S. Sharma, S. C. Barman, H. Yoon, S. Ko, C. Park, S. Yoon, H. Kim, J. Y. Park, *Adv. Funct. Mater.* **2021**, *31*, 2007661.

[182] Z. Wan, S. Wang, B. Haylock, Z. Wu, T. K. Nguyen, H. P. Phan, R. Sang, N. T. Nguyen, D. Thiel, S. Koulakov, A. Trinchi, *Adv. Mater. Technol.* **2021**, *6*, 2001191.

[183] M. Hepp, H. Wang, K. Derr, S. Delacroix, S. Ronneberger, F. F. Loeffler, B. Butz, V. Strauss, *npj Flex. Electron.* **2022**, *6*, 3.

[184] Q. Du, L. Liu, R. Tang, J. Ai, Z. Wang, Q. Fu, C. Li, Y. Chen, X. Feng, *Adv. Mater. Technol.* **2021**, *6*, 2100122.

[185] S. Duan, Y. Lin, Z. Wang, J. Tang, Y. Li, D. Zhu, J. Wu, L. Tao, C. H. Choi, L. Sun, J. Xia, *Research* **2021**, *2021*, 9861467.

[186] W. Hu, Y. Li, S. Y. Tang, L. Li, Q. J. Niu, S. Yan, *Adv. Mater. Interfaces* **2021**, *8*, 2100038.

[187] X. Liu, S. Lebedkin, H. Besser, W. Pfleging, S. Prinz, M. Wissmann, P. M. Schwab, I. Nazarenko, M. Guttmann, M. M. Kappes, U. Lemmer, *ACS Nano* **2015**, *9*, 260.

[188] B. Han, Y. L. Zhang, L. Zhu, X. H. Chen, Z. C. Ma, X. L. Zhang, J. N. Wang, W. Wang, Y. Q. Liu, Q. D. Chen, H. B. Sun, *Sensor Actuat. B-Chem.* **2018**, *270*, 500.

[189] O. Parlak, S. T. Keene, A. Marais, V. F. Curto, A. Salleo, *Sci. Adv.* **2018**, *4*, eaar2904.

[190] S. K. Arya, P. Kongsuphol, M. K. Park, *Biosens. Bioelectron.* **2017**, *92*, 542.

[191] F. Tehrani, B. Bavarian, *Sci. Rep.* **2016**, *6*, 27975.

[192] Y. Lei, A. H. Alshareef, W. Zhao, S. Inal, *ACS Appl. Nano Mater.* **2019**, *3*, 1166.

[193] Y. Yang, Y. Song, X. Bo, J. Min, O. S. Pak, L. Zhu, M. Wang, J. Tu, A. Kogan, H. Zhang, T. K. Hsiai. *Nat. Biotechnol.* **2020**, *38*, 217.

[194] R. M. Torrente-Rodríguez, J. Tu, Y. Yang, J. Min, M. Wang, Y. Song, Y. Yu, C. Xu, C. Ye, W. W. IsHak, W. Gao, *Matter* **2020**, *2*, 921-937.

[195] H. Yoon, J. Nah, H. Kim, S. Ko, M. Sharifuzzaman, S. C. Barman, X. Xuan, J. Kim, J. Y. Park, *Sensor. Actuat. B-Chem.* **2020**, *311*, 127866.

[196] R. R. Soares, R. G. Hjort, C. C. Pola, K. Parate, E. L. Reis, N. F. Soares, E. S. McLamore, J. C. Claussen,

C. L. Gomes, *ACS Sens.* **2020**, *5*, 1900-1911.

[197] J. Zhu, S. Liu, Z. Hu, X. Zhang, N. Yi, K. Tang, M. G. Dexheimer, X. Lian, Q. Wang, J. Yang, J. Gray, *Biosens. Bioelectron.* **2021**, *193*, 113606.

[198] W. He, C. Wang, H. Wang, M. Jian, W. Lu, X. Liang, X. Zhang, F. Yang, Y. Zhang, *Sci. Adv*. **2019**, *5*, eaax0649.

[199] Q. Gao, W. Zhang, C. Zhao, W. Yan, S. Han, Y. Li, Q. Liu, X. Li, D. Liu, *Adv. Mater. Interfaces* **2022**, *9*, 2200034.

[200] R. M. Torrente-Rodríguez, H. Lukas, J. Tu, J. Min, Y. Yang, C. Xu, H. B. Rossiter, W. Gao, *Matter* **2020**, *3*, 1981.

[201] C. Muratore, M. K. Muratore, D. R. Austin, P. Miesle, A. K. Benton, L. K. Beagle, M. J. Motala, D. C. Moore, J. M. Slocik, M. C. Brothers, S. S. Kim, *Adv. Mater. Interfaces* **2022**, *9*, 2102209.

[202] J. Li, X. Bo, *J. Hazard. Mater.* **2022**, *423*, 127014.

[203] Y. Jung, J. Min, J. Choi, J. Bang, S. Jeong, K. R. Pyun, J. Ahn, Y. Cho, S. Hong, S. Hong, J. Lee, *Appl. Mater. Today* **2022**, *29*, 101589.

[204] R. R. Gattass, E. Mazur, *Nat. Photon.* **2008**, *2*, 219.